Detectors in Nuclear and Particle Physics

Prof. Dr. Johanna Stachel

Department of Physics und Astronomy
University of Heidelberg

May 8, 2018

3. Gas Detectors

3.1 General introduction

Principle

- ionizing particle creates primary and secondary charges via energy loss by ionization (Bethe-Bloch, chapter 2) N_0 electrons and ions
- charges drift in electric field
- generally gas amplification in the vicinity of an anode wire
- signal generation

different operation modes depending on electric field strength

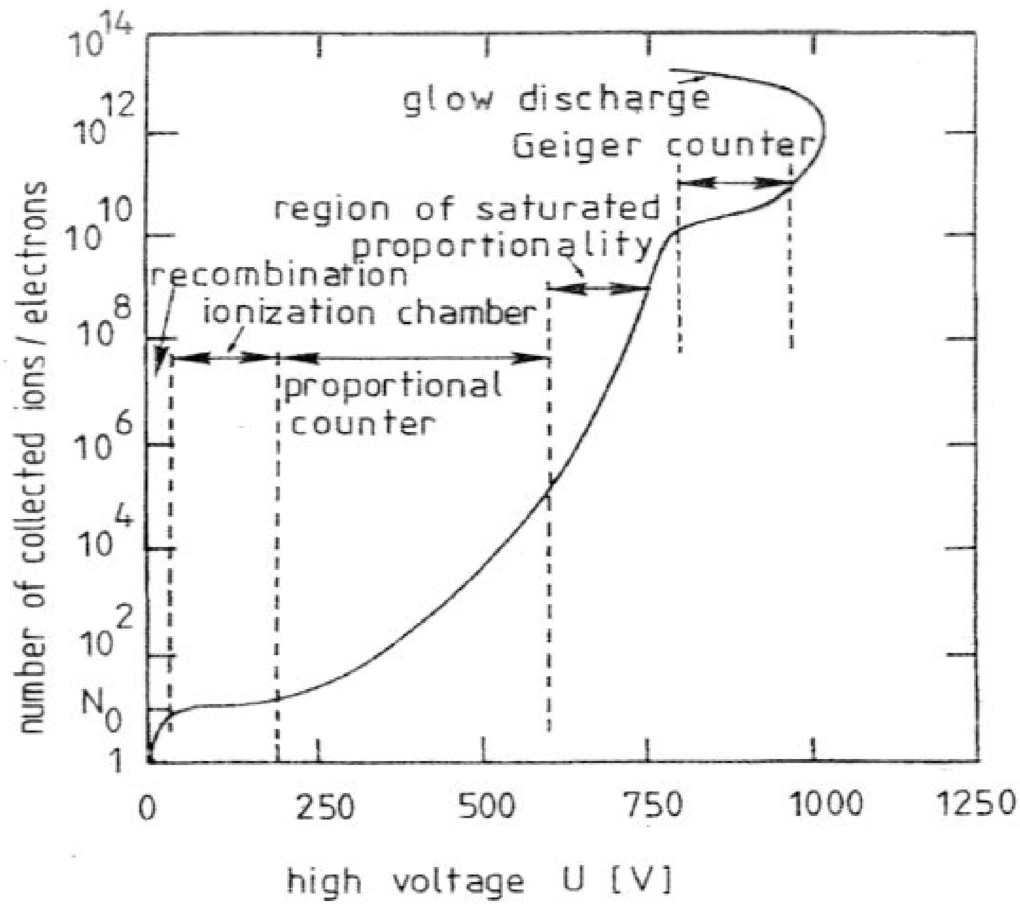

modes of operation of gas detectors (after F. Sauli 1977, lecture notes)

Charge carriers in layer of thickness L for a mean energy W to produce electron-ion pair

- mean number:

$$\langle n_t \rangle = \frac{L \langle \frac{dE}{dx} \rangle_{\text{ion}}}{W}$$

  about $2-6$ times the primary number (see chapter 2)
  important for spatial resolution: secondary ionization by δ-electrons happens on length scale 10 μm
  e.g. $T_e = 1$ keV in iso-butane $\rightarrow R = 20\ \mu m$

- ionization statistics:
  $\lambda = 1/\sigma_I \rho$ mean distance between ionization events with cross section σ_I
  mean number of ionization events $\langle n \rangle = L/\lambda$

Poisson distribution about mean $\langle n \rangle$

$$P(n, \langle n \rangle) = \frac{\langle n \rangle^n \exp(-\langle n \rangle)}{n!}$$

and specifically probability for **no** ionization

$$P(0, \langle n \rangle) = \exp(-\langle n \rangle) = \exp(-L/\lambda)$$

efficiency of gas detectors allows determination of λ and hence σ_I
typical values:

	λ (cm)
He	0.25
air	0.053
Xe	0.023

$\rightarrow \sigma_I = 10^{-22}$ cm^2 or 100 b

3.2 Charge Transport
- Ion mobility

Ions drift along field lines in external E-field with superimposed random thermal motion
ion transfers in collisions with gas atoms typically half of its energy $\rightarrow$ kinetic energy of ion is approximately thermal energy

$$\langle T_{\text{ion}}(\vec{E})\rangle \simeq \langle T_{\text{ion}}(\text{therm})\rangle = \frac{3}{2}kT$$

drift velocity in direction of $\vec{E}$: develops from one collision to the next (thermal velocity has random orientation relative to $\vec{E}$)
assume instantaneous ion velocity due to electric field $u_e = 0$ at $t = 0$ and typical collision time τ

$\rightarrow$ directly prior to collision $\quad \vec{u}_e = \vec{a}\cdot\tau = \dfrac{e\vec{E}}{M}\cdot\tau$

$\rightarrow$ drift velocity of ion $\quad \vec{v}_{D^+} = \langle\vec{u}_e\rangle = \dfrac{1}{2}u_e = \dfrac{e\vec{E}}{2M}\tau = \mu_+\vec{E} \qquad \boxed{\mu_+ \equiv \text{ion mobility}}$

where $\tau \propto \lambda \propto 1/\sigma_+ \simeq$ constant since $\langle T_{\text{ion}}\rangle$ essentially thermal.

e.g. $C_4H_{10}^+$ in C_4H_{10} $\quad \mu_+ = 0.61\,\dfrac{\text{cm/s}}{\text{V/cm}}$ at $E = 1$ kV/cm $\rightarrow v_{D^+} = 0.6$ cm/ms
typical drift distances cm $\rightarrow$ typical ion drift times ms

Electron mobility I

In a constant E-field, electrons drift towards anode of a gas detector with a constant velocity, measurement of drift time allows to determine point of ionization.

$$\Delta t = \frac{L}{v_D}$$

equation of motion of electron in superimposed $\vec{E}$ and $\vec{B}$-fields (Langevin):

$$m\frac{\mathrm{d}\vec{v}}{\mathrm{d}t} = e\vec{E} + e(\vec{v} \times \vec{B}) + \vec{Q}(t)$$

with instantaneous velocity $\vec{v}$ and a stochastic, time dependent term $Q(t)$ due to collisions with gas atoms

assume: collision time τ
$\vec{E}$ and $\vec{B}$ constant between collisions
consider $\Delta t \gg \tau$ (averaging) $\rightarrow Q(t)$ is friction

steady state is reached when net force is zero, defines drift velocity v_D

$$\langle m\frac{d\vec{v}}{dt}\rangle = e(\vec{E} + \vec{v}_D \times \vec{B}) - \underbrace{\frac{m}{\tau}\vec{v}_D}_{\text{Stokes-type}} = 0$$

Electron mobility II

$B = 0$: $\quad \vec{v}_D = \mu_- \vec{E} \quad$ with $\quad \mu_- = \dfrac{e\tau}{m} \equiv \mu$

$B \neq 0$: $\quad \vec{v}_D = \mu_- \vec{E} + \omega\tau(\vec{v}_D \times \vec{B}) \quad$ with Larmor frequency $\omega = \dfrac{eB}{m}$ (see below)

Compared to ions, $\mu_+ \ll \mu_-$ since $M \gg m$

2 types of gases

a) hot gases: atoms with few low-lying levels, electron loses little energy in a collision with atom $\rightarrow T_e \gg kT$
acceleration in E-field and friction lead to constant v_D for a given $\vec{E}$
'free fall with friction'
but $\quad \lambda(T_e) \simeq \lambda(|\vec{E}|)$ and
$\mu \propto \tau \propto 1/\sigma(|\vec{E}|)$ not constant.

typical drift velocity: $v_D = 3 - 5$ cm$/\mu$s for 90% Ar/10% CH_4 (typically saturating with E)

b) cold gases: many low-lying degrees of freedom
$\rightarrow$ electrons lose kinetic energy they gain in between collisions (similar to ions)
$T_e \simeq kT \qquad \mu \simeq$ constant $\qquad v_D \propto |E|$

examples: Ar/CO_2 or Ne/CO_2

in latter: $\mu \simeq 7.0 \cdot 10^{-3}$ cm$^2/\mu$s V at 10% CO_2 $\quad$ or $v_D = 2$ cm$/\mu$s at 300 V/cm
$3.5 \cdot 10^{-3}$ cm$^2/\mu$s V at 20% $\quad v_D = 1$ cm$/\mu$s

Electron mobility III

Drift in combined $\vec{E}$ and $\vec{B}$-fields

$$\vec{v}_D = \frac{\mu|\vec{E}|}{1+\omega^2\tau^2}[\hat{E} + \underbrace{\omega\tau\hat{E}\times\hat{B}}_{\substack{\text{component}\\ \text{in direction}\\ \vec{E}\times\vec{B}\\ \propto\,\omega\tau}} + \underbrace{\omega^2\tau^2(\hat{E}\cdot\hat{B})\hat{B}}_{\substack{\text{component}\\ \text{in direction}\\ \vec{B}\\ \propto\,(\omega\tau)^2}}]$$

$\hat{E}$, $\hat{B}$: unit vectors in direction of E- and B-field

Electron loss

with some probability a free electron is lost during drift

a) recombination $\text{ion}^+ + e^-$

decrease in number of negative (and positive) charge carriers

$$-\frac{dN^-}{dt} = p_r \cdot \rho^+ \rho^- \qquad p_r : \text{coefficient of recombination} \simeq 10^{-7}\ \text{cm}^3/\text{s}$$

generally not important

b) electron attachment

on electro-negative molecules, probability can be large

$$e^- + M \rightarrow M^- \qquad \text{for } T_e \simeq 1\ eV$$

otherwise dissociative attachment

$$e^- + XY \rightarrow X + Y^-$$

for gases like O_2, Cl_2, freon, SF_6 probability per collision is of order 10^{-4}

capture coefficient p_c is strongly energy dependent (in many gases there is a minimum around 1 eV, large transparency for slow electrons 'Ramsauer effect')

electron undergoes order of 10^{11} collisions/s $\rightarrow$ for drift time of 10^{-6} s fraction lost x_{loss} depends on partial oxygen pressure

$$x_{\text{loss}} = 10^{-4} \cdot (10^{11}/\text{s}) \cdot (10^{-6}\ \text{s}) \cdot P_{O_2}/P_{\text{atm}}$$

$\rightarrow$ less than 1% lost for $P_{O_2}/P_{\text{atm}} \leq 10^{-3}$

Remark: in presence of certain quencher gases such as CO_2 the effect of O_2 is enhanced by multistep catalytic reaction

- 10 ppm O_2 can lead to 10% loss within 10 μs $\rightarrow$ need to keep oxygen level low in gas.

Diffusion I

Original ionization trail diffuses (spreads apart) with drift time
$\rightarrow$ effect on space point and momentum resolution, ultimate limit

a) only thermal motion ($|\vec{E}| = |\vec{B}| = 0$)
mean thermal velocity

$$\langle v \rangle = \frac{\lambda}{\tau}$$
$$\langle T_e \rangle = \frac{1}{2} m \langle v \rangle^2$$

λ mean free path
τ time between collisions

for a point-like source at time $t = 0$, collisions between electrons and gas atoms (molecules)
$\rightarrow$ smearing: spread of charge cloud at time of first collision

$$R^2 = 2\lambda^2$$

and after $n = t/\tau$ collisions

$$\sigma^2(t) = 2\lambda^2 t/\tau$$

define diffusion coefficient $\quad D = \dfrac{\sigma^2(t)}{2t}$

for $|\vec{E}| = |\vec{B}| = 0 \quad D = D_0 = \dfrac{\lambda_0^2}{\tau} = \dfrac{2\langle T_e \rangle}{m}\tau$

Diffusion II

diffusion is isotropic

longitudinal diffusion coefficient $D_{0L} = \frac{1}{3}\frac{\lambda_0^2}{\tau}$

transverse diffusion coefficient $D_{0T} = \frac{2}{3}\frac{\lambda_0^2}{\tau}$

$\rightarrow$ after time t charge cloud has width $\sigma(t) = \sqrt{D2t}$

respectively, in each dimension $\sigma_x(t) = \sigma_y(t) = \sigma_z(t) = \sqrt{\frac{1}{3}D2t}$

charge distribution Gaussian $N(x) = c \cdot \exp(-\frac{x^2}{2\sigma_x^2})$

diffusion equation: charge density $\rho(\vec{r}, t)$ for conserved electron current $\vec{j}$ defined by

$$\frac{\partial \rho}{\partial t} + \nabla \cdot \vec{j} = 0$$

without field, $\vec{j} = -D\nabla\rho \Rightarrow \frac{\partial \rho}{\partial t} = D\Delta\rho$

solved by $\rho(\vec{r}, t) = c \cdot \exp(-\frac{\vec{r}^2}{4Dt})$

Diffusion III

hot gases: $\langle T_e \rangle \gg \frac{3}{2} kT$ $\quad D$ large

cold gases: $\langle T_e \rangle \simeq \frac{3}{2} kT$ $\quad D$ small

with 1-dim diffusion coeff. $D = \dfrac{2\langle T_e \rangle}{3m} \tau$

and $\quad \mu = \dfrac{e}{m} \tau \qquad$ (B=0)

$$\langle T_e \rangle = \frac{3}{2} e \frac{D}{\mu}$$

can define a characteristic energy

$$\epsilon_k = \frac{2}{3} \langle T_e \rangle = e \frac{D}{\mu}$$

diffusion of cloud after distance L

$$\sigma_x^2 = 2Dt = 2D \frac{L}{\mu E} = \frac{2\epsilon_k}{eE} L \tag{1}$$

for hot gas the same characteristic energy is reached at much lower T

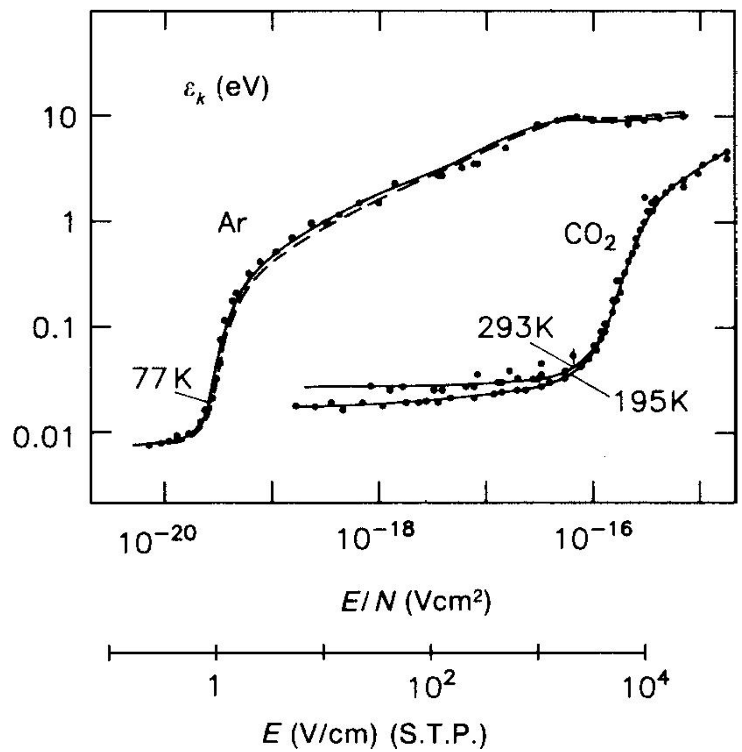

characteristic energy of electrons in Ar and CO_2 as a function of the reduced E. The electric field under normal conditions is also indicated. The parameters refer to temperatures at which the measurements were made.

Diffusion IV

b) diffusion in B-field

$$\vec{B} = B\vec{e}_z$$

along B no Lorentz force

$D_L(B) = D_{0L} = \frac{1}{3} D_0$

in transverse direction Lorentz force helps to keep charge cloud together, i.e. it counteracts diffusion

$$D_T(B) = \frac{D_{0T}}{1 + \omega^2 \tau^2}$$

for $\vec{B}$ large

$\rightarrow \omega\tau \gg 1 \qquad D_T(B) \ll D_{0T}$

e.g. Ar/CH_4 at $B = 1.5\ T$

$$D_T(1.5\ T) \simeq \frac{1}{50} D_{0T}$$

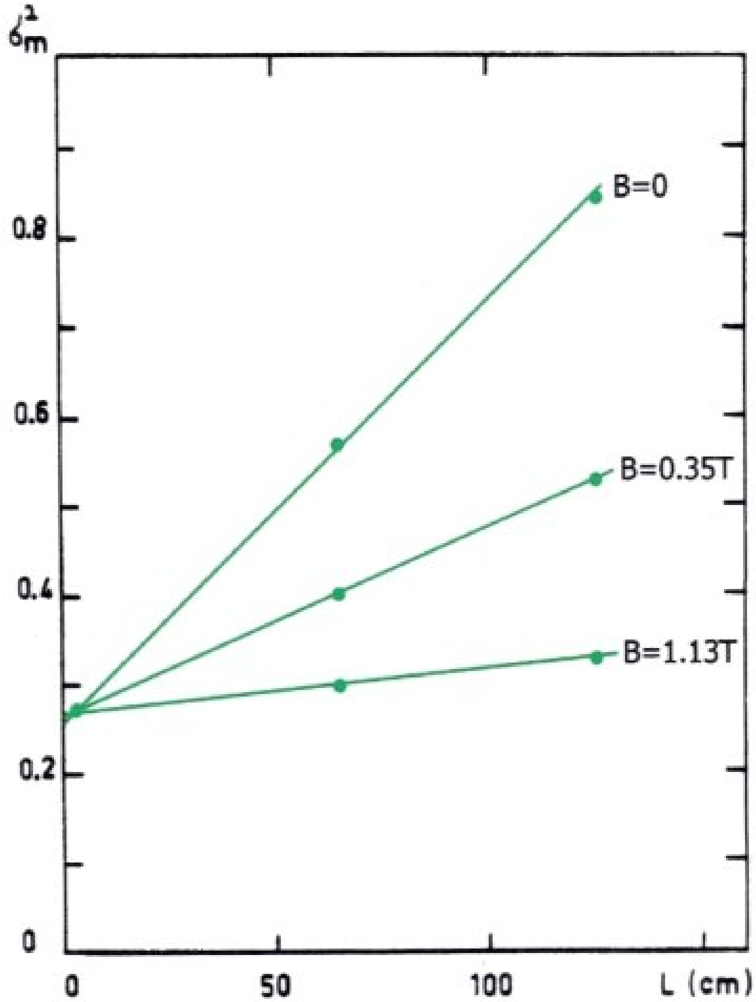

transverse σ^2 as function of L

Diffusion V

c) diffusion in E-field:
ordered drift along field superimposed to statistical diffusion
mobility μ is function of $\langle T_e \rangle$

$$\vec{v}_D = \mu(\langle T_e \rangle) \cdot \vec{E}$$

$\rightarrow$ energy spread leads to longitudinal spreading of electron cloud $D_L \neq \frac{1}{2} D_T$

statistical transverse diffusion not affected by E-field

in hot gases:
for large E, $D_L > D_T$ and values are large

in cold gases: $D_L \simeq D_T$ small

$$\sigma^2(t) = 2Dt = 2D\frac{L_D}{v_D} = \frac{2kT}{e|\vec{E}|}L_D$$

$$\frac{\sigma^2(t)}{L_D} = \frac{2kT}{e|\vec{E}|}$$

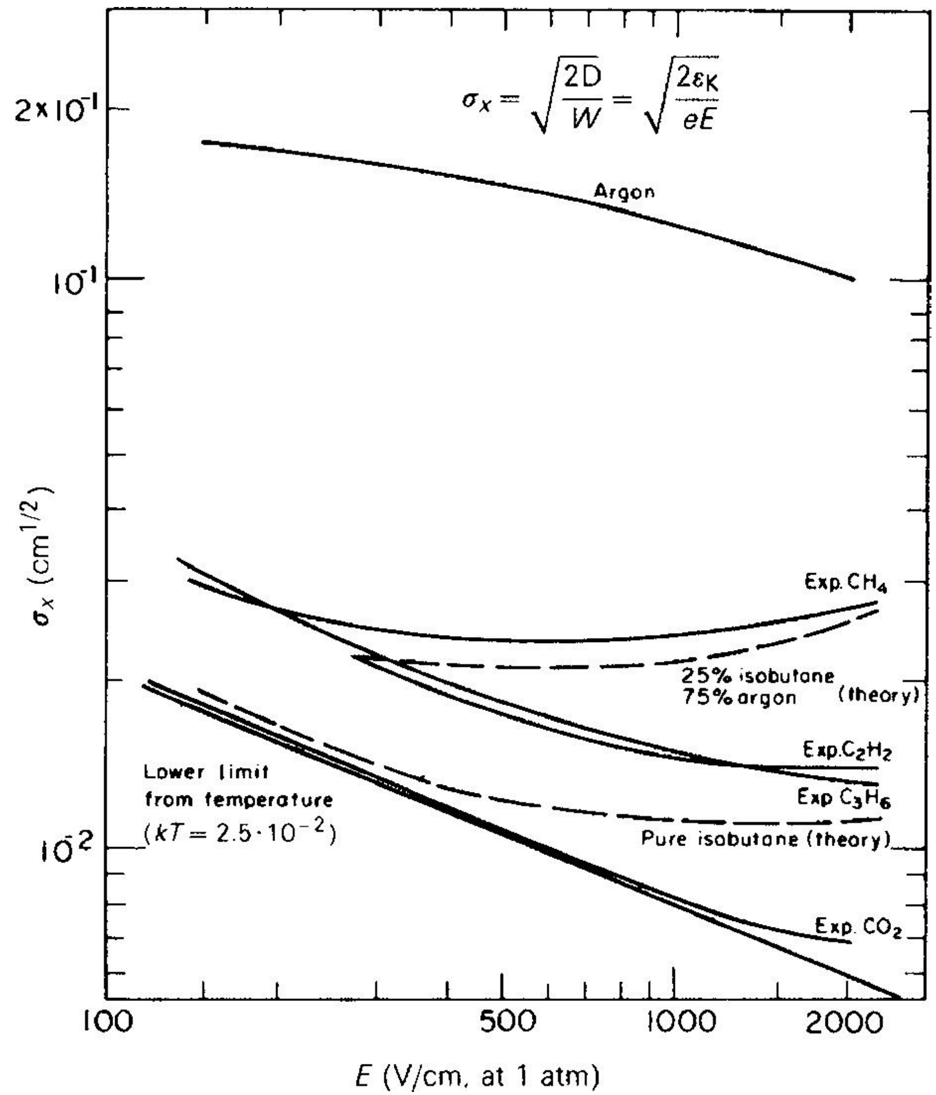

longitudinal diffusion width $\sigma_x/\sqrt{L_D}$ after 1 cm of drift

Exact solution

of drift and diffusion by solving a 'transport equation' for electron density distribution $f(t, \vec{r}, \vec{v})$

Boltzmann-equation:

$$\frac{\partial f}{\partial t} + \underbrace{\vec{v}\frac{\partial}{\partial \vec{r}} f}_{\text{flow term}} + \underbrace{\frac{\partial}{\partial \vec{v}}\vec{g}}_{\text{external forces}} = \underbrace{Q(t)}_{\text{collision term (stochastic)}}$$

$$\vec{g} = \left(\frac{e\vec{E}}{m} + \vec{\omega} \times \vec{v}\right) f$$

numerical solution with codes such as Magboltz & Garfield

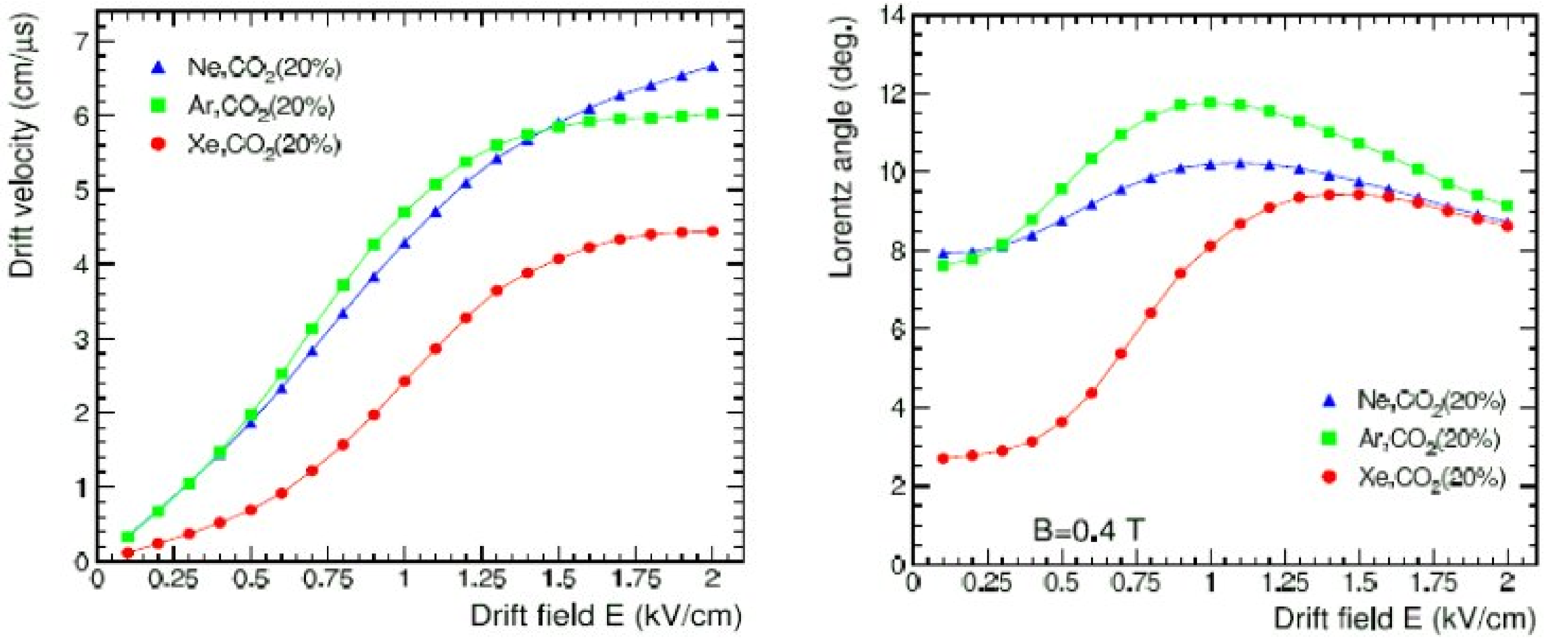

Lorentz angle: angle between E-field and drift velocity of electrons in presence of B not $\perp$ to E

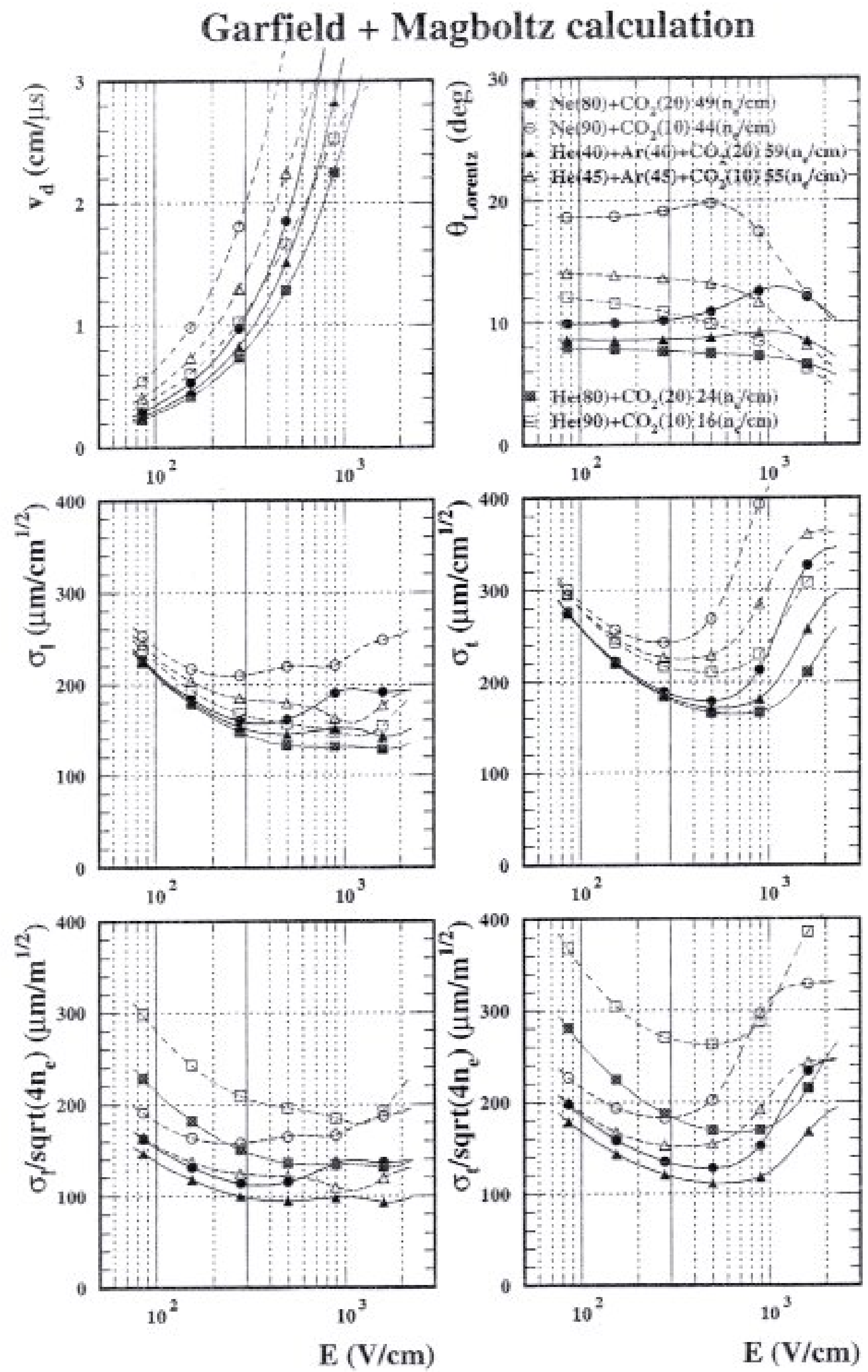

Drift velocity (top left), Lorentz angle (top right), longitudinal and transverse diffusion constants (middle) and longitudinal and transverse diffusion constants normalized to the square root of the number of charge carriers (bottom) for different mixtures of noble gas and CO_2.

Lorentz angle: angle between E-field and drift velocity of electrons in presence of B not $\perp$ to E

3.3 Gas amplification

in case the anode is a (thin) wire, E-field in vicinity of wire very large $E \propto 1/r$ and the electron gains large kinetic energy.

$$\begin{aligned}
\Delta T_e &= e\Delta U \\
&= e\int_{r_1}^{r_2} E(r)\mathrm{d}r \\
&= \frac{eU_o}{\ln r_o/r_i}\int_{r_1}^{r_2}\frac{1}{r}\mathrm{d}r \\
&= eU_o\frac{\ln r_2/r_1}{\ln r_o/r_i}
\end{aligned}$$

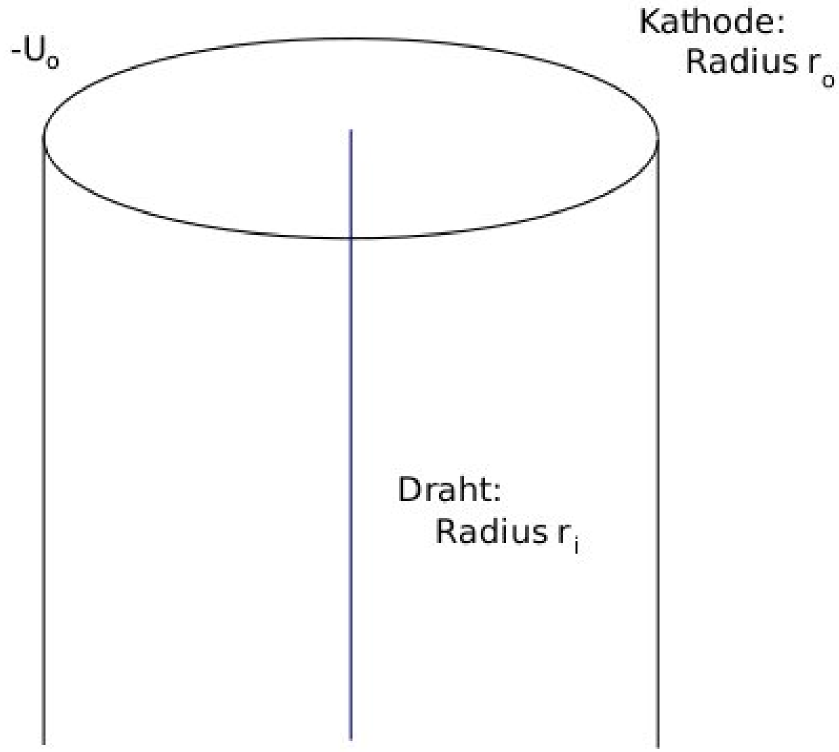

in order to obtain large E and hence large ΔT_e, use very thin wires ($r_i \simeq 10 - 50\ \mu m$)
within few wire radii, ΔT_e becomes large enough for secondary ionization
strong increase of $E \rightarrow$ avalanche formation for $r \rightarrow r_i$.

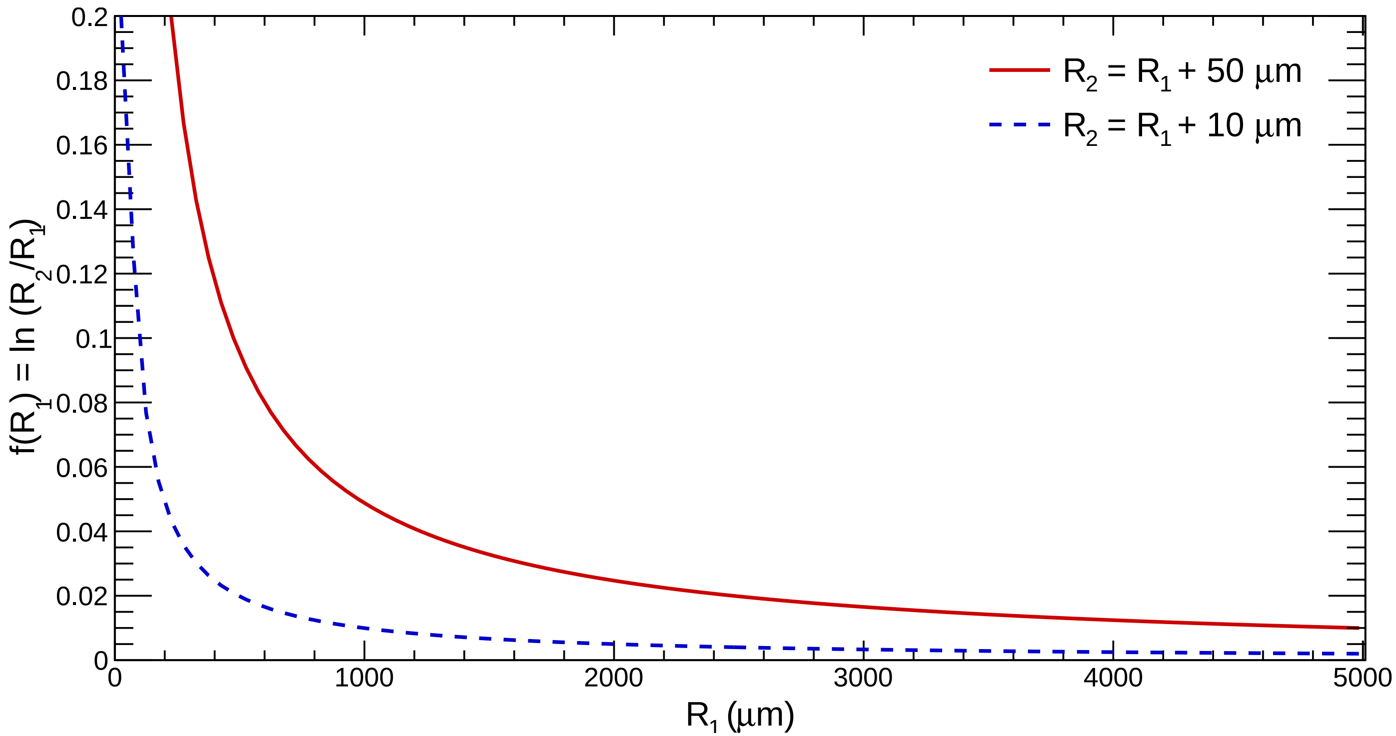

Avalanche formation in vicinity of a thin wire

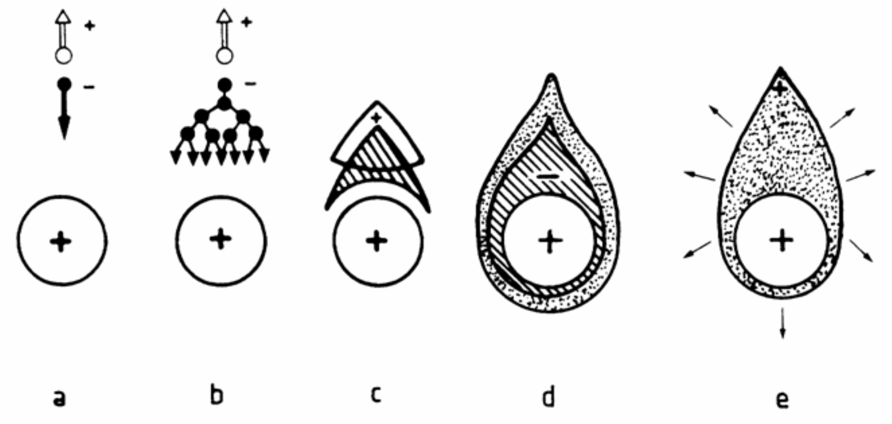

Temporal and spatial development of an electron avalanche

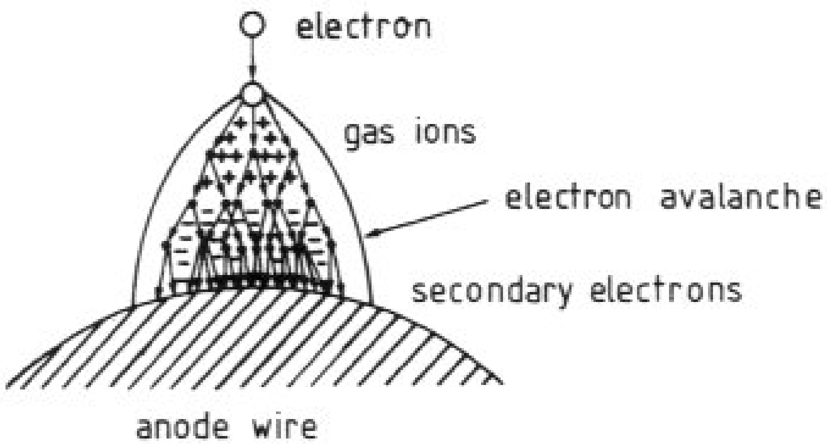

Illustration of the avalanche formation on an anode wire in a proportional counter. By lateral diffusion a drop-shaped avalanche develops.

Photographic reproduction of an electron avalanche. The photo shows the form of the avalanche. It was made visible in a cloud chamber by droplets which have condensed on the positive ions.

First Townsend coefficient α

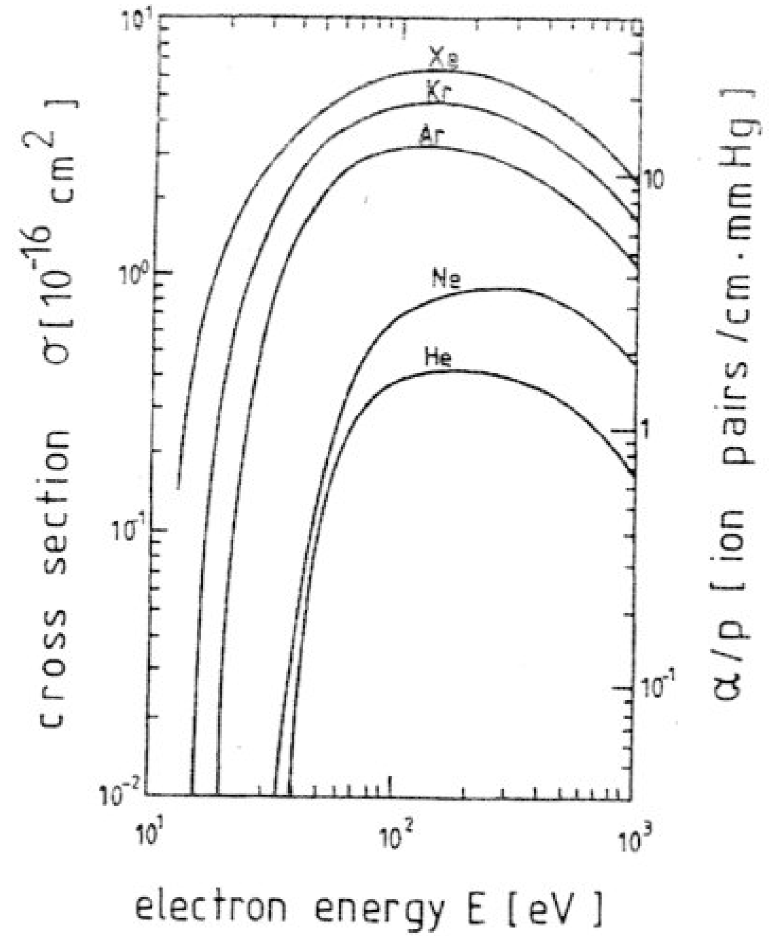

Energy dependence of the cross section for ionization by collision.

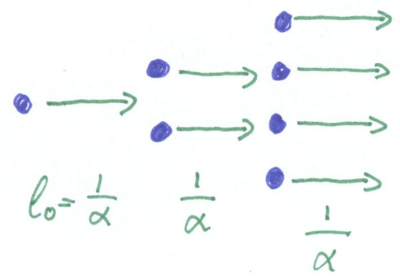

number of electrons $N(x) = N_0 \underbrace{\exp \alpha x}_{\text{gas gain}}$

mean free path $l_0 = 1/\alpha = 1/(N\sigma(T_e))$

$T_e = T_e(E(x))$

$\Rightarrow \alpha = \alpha(x)$

gas gain $G = \exp\left(\int_{r_1}^{r_2} \alpha(x)\, dx \right)$

typically $10^4 - 10^5$, up to 10^6 possible in proportional mode.
limit: discharge (spark) at $\alpha x \simeq 20$
or $G = 10^8$ 'Raether-limit'

Second Townsend coefficient

excitation of gas generates UV-photons which in turn can lead to photo effect in gas and on cathode wire, contributing thus to avalanche.

$$\gamma = \frac{\#\ \text{photo effect events}}{\#\ \text{avalanche electrons}}$$

gas gain including photo effect

$$G_\gamma = \underbrace{G}_{\text{no}} + \underbrace{G(G\gamma)}_{\text{one}} + \underbrace{G(G\gamma)^2}_{\text{two}} + \ldots = \frac{G}{1-\gamma G}$$

photo effect events

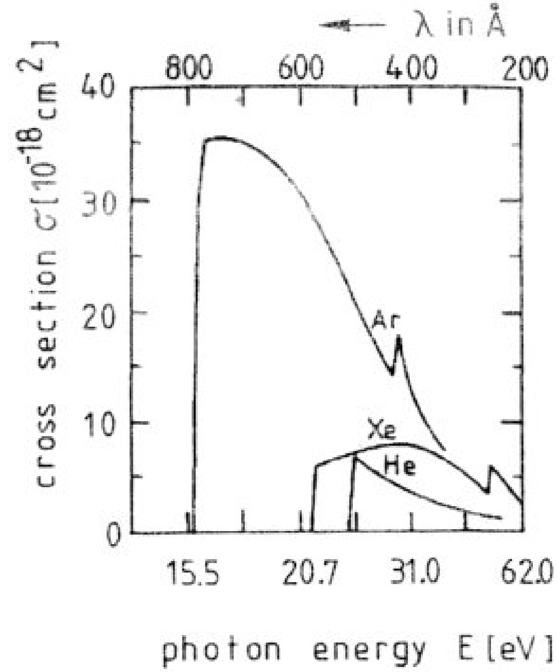

Energy dependence of the cross section for photoionization

limit: $\gamma G \to 1$ continuous discharge independent of primary ionization

to prevent this, add to gas so-called quench-gas which absorbs UV photons strongly, leading to excitation and radiationless transitions

examples: CH_4, C_4H_{10}, CO_2

3.4 Ionization chamber

no gas gain, charges move in electric field and induce signal in electrodes.

2 electrodes form parallel plate capacitor.

consider motion of a free charge q: electric field does work, capacitor is charged (lowering in energy of capacitor).

$$q\vec{\nabla}\Phi \cdot \; d\vec{x} \quad = \quad dq_i \cdot U_0$$

leads to induced current

$$I_{\mathrm{ind}} \quad = \quad \frac{q}{U_0}\vec{\nabla}\Phi \cdot \vec{v_D}$$

$$\text{with } \vec{E} \quad = \quad -\vec{\nabla}\Phi \text{ and } U_0 = \Phi_1 - \Phi_2$$

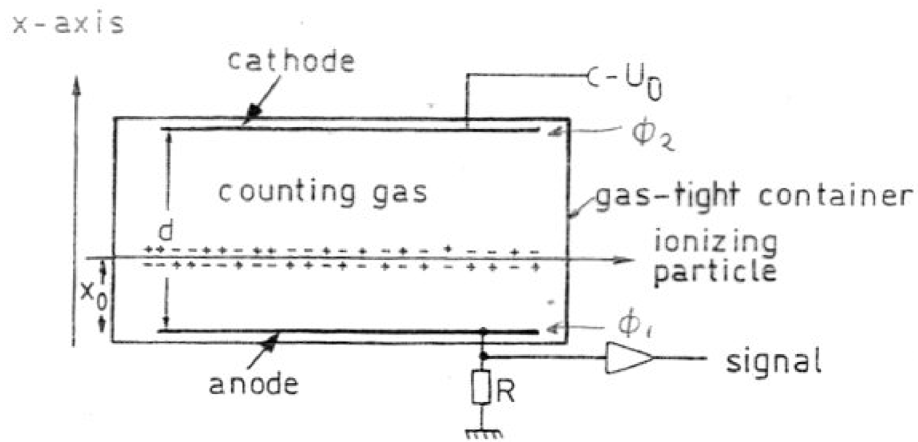

Principle of operation of a planar ionization chamber

- current is constant **while** charge is drifting
- total induced signal (charge) independent of x_0
- signal induced by electrons $$\Delta q_- = \frac{N_e}{U_0}(\Phi(x_0) - \Phi_1)$$
- signal induced by ions $$\Delta q_+ = -\frac{N_e}{U_0}(\Phi(x_0) - \Phi_2)$$
- $|N_{ion}| = |N_e|$, but opposite charge $\rightarrow$ total $\Delta q = \Delta q_- + \Delta q_+ = N_e$

practical problem: ion comparatively slow $w_+ = 10^{-3} \dots 10^{-2} w_-$ (see mobilities above)
(except for semiconductors: typ. $w_+ \approx 0.5\ w_-$)

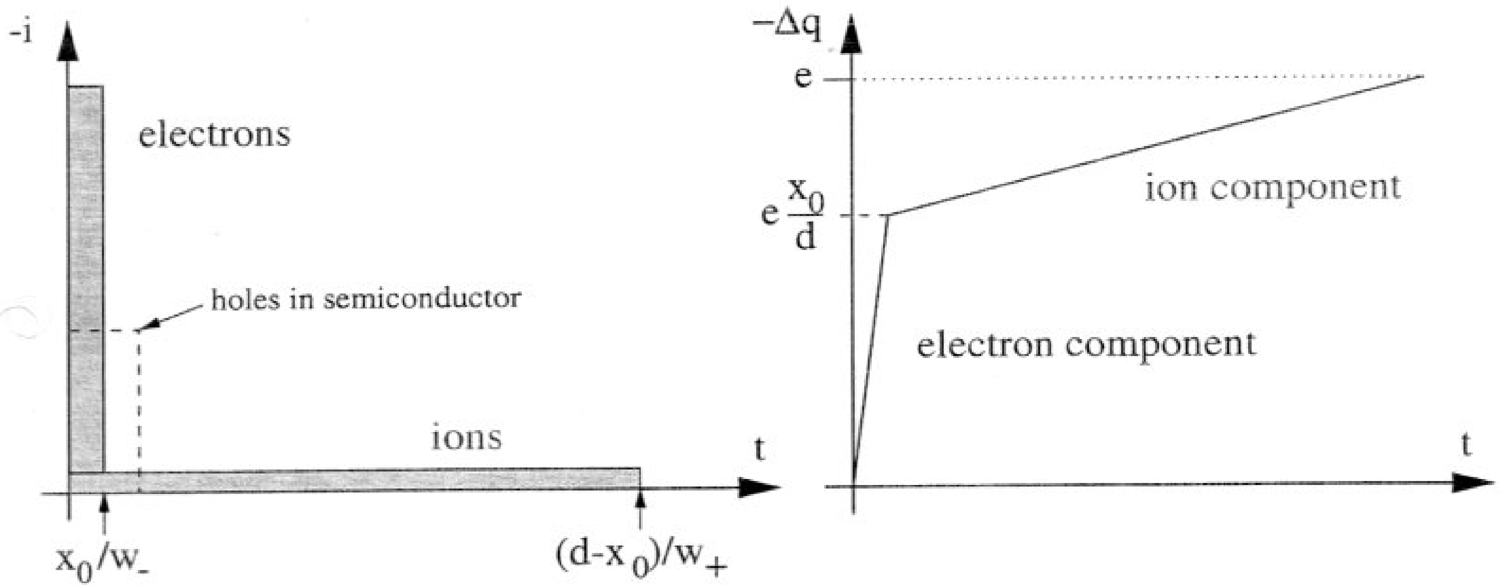

Induced current and charge for parallel plate case, ratio w_-/w_+ decreased for purpose of illustration.

signal generated during drift of charges

- induced current ends when charges reach electrodes
- induced charge becomes constant (total number N_e)
- signal shaping by differentiation (speed of read-out) $\rightarrow$ suppresses slow ion component

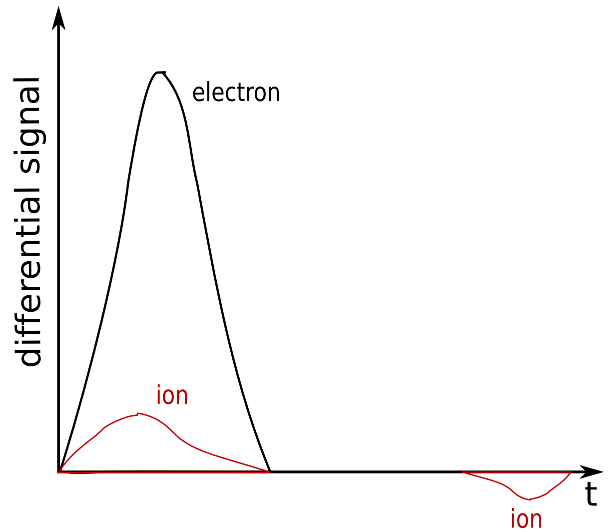

change in potential $dU = \frac{\mathrm{d}Q}{C}$
U_0 = external voltage
typical time constant of power supply (+ cables ...)

$RC \gg \Delta t^-, \Delta t^+$

usually electronic signal shaping needed

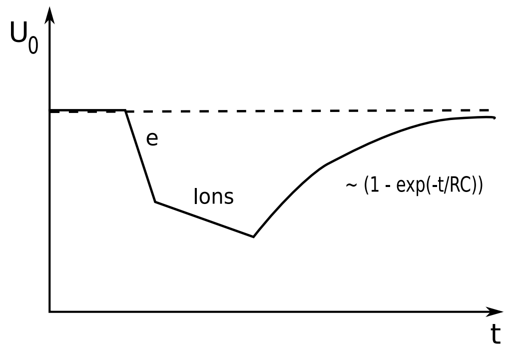

Signal shaping by RC-filter

choose e.g. $\Delta t^- \ll RC \ll \Delta t^+$
damps ion component

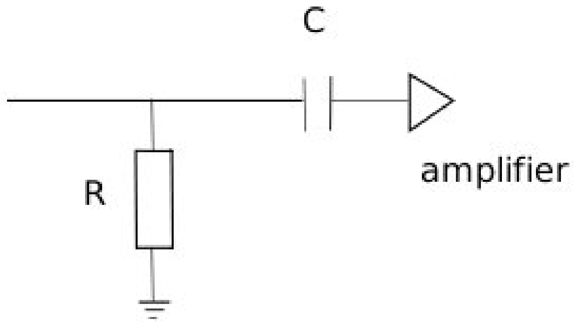

$$\begin{aligned}\Delta U &= \Delta U^- + \Delta U^+ \\ &= \frac{\Delta Q^-}{C} + \frac{\Delta Q^+}{C}\end{aligned}$$

where ΔQ^{+-} is the charge induced in the anode by motion of ions and electrons for total number of ionization events in gas N_e

$$\begin{aligned}
\Delta Q^- &= N_e \frac{\Phi(x_0) - \Phi_1}{U_0} \\
&= N_e \frac{x_0}{d} \\
\Delta Q^+ &= -N_e \frac{\Phi(x_0) - \Phi_2}{U_0} \\
&= N_e \frac{d - x_0}{d} \\
\text{without filter} \quad \Delta Q &= N_e, \qquad \Delta U = \frac{N_e}{C} \\
\text{with filter} \quad d - x_0 &= v^+ \Delta t^+ \\
&\rightarrow \underbrace{v^+ RC \left(1 - \exp(-\frac{\Delta t^+}{RC})\right)}_{\text{damping of ion component}}
\end{aligned}$$

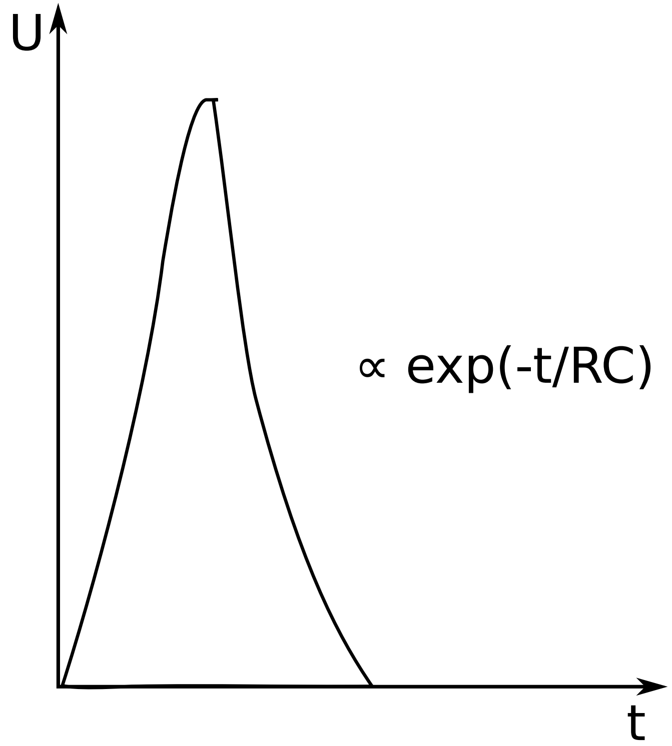

fast rise and decrease of signal but now pulse height depends on x_0

trick: introduce additional grid, the "Frisch grid"
while electrons drift towards Frisch grid, no induced signal on anode, only on Frisch Grid
as soon as electrons pass Frisch grid, signal induced on anode
choose U_g such that the E-field is unchanged

$$\Delta Q = \Delta Q^- = N_e$$
$$\Delta t^- = \frac{d_g}{v^-}$$

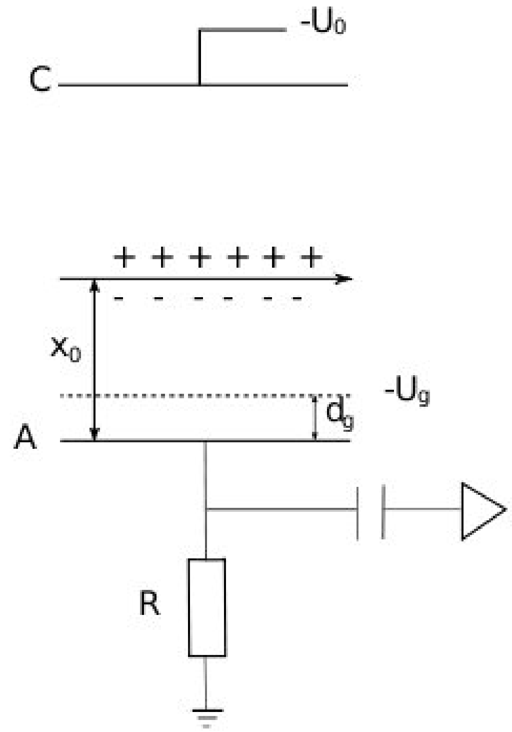

general difficulty for ionization chambers: small signals
example: 1 MeV particle stops in gas

$$\begin{aligned} N_e &\simeq \frac{10^6 \text{ eV}}{35 \text{ eV}} \simeq 3 \cdot 10^4 \\ C &\simeq 100 \text{ pF} \\ \Rightarrow \Delta U_{max} &= \frac{3 \cdot 10^4 \cdot 1.6 \cdot 10^{-19} \text{ C}}{10^{-10} \text{ F}} \\ &= 4.6 \cdot 10^{-5} \text{ V} \end{aligned}$$

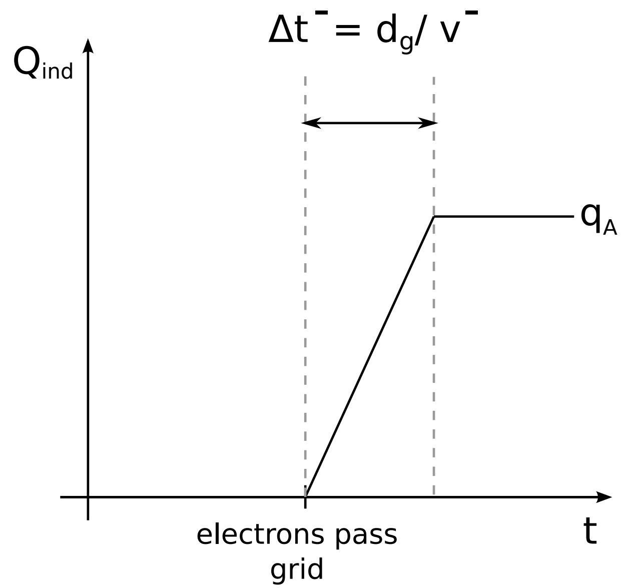

need sensitive, low-noise preamplifier

application: e.g. cylindrical ionization chamber for radiation dosimetry

$$\vec{E}(r) = -\frac{U_0}{r \ln r_a/r_i}\hat{e}_r$$

ionization at radius r_0:

$$\begin{aligned} \Delta t^- &= \int_{r_0}^{r_i} \frac{\mathrm{d}r}{v^-(r)} = -\int \frac{\mathrm{d}r}{\mu^- E} \\ &= -\int_{r_0}^{r_i} \frac{dr}{\mu^- U_0} r \ln \frac{r_a}{r_i} \\ &= \frac{\ln(r_a/r_i)}{2\mu^- U_0}(r_0^2 - r_i^2) \end{aligned}$$

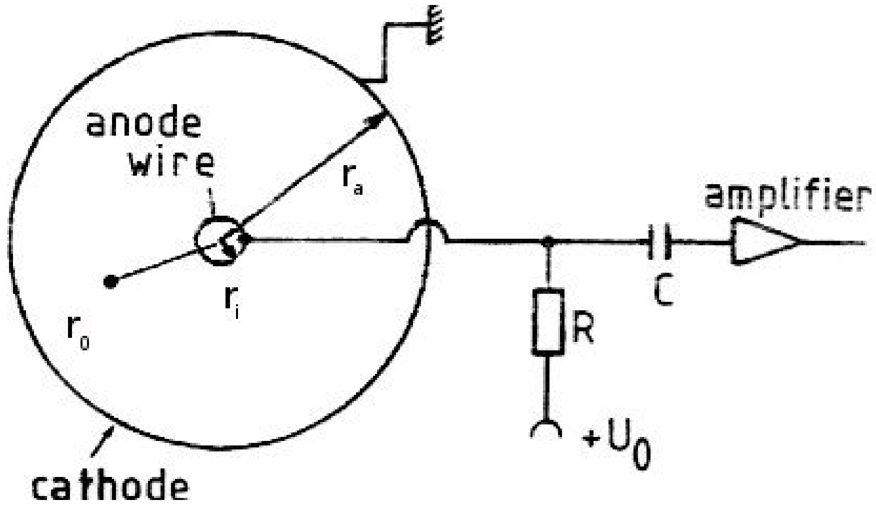

Principle of operation of a cylindrical ionization chamber

l_0: typical ionization length, the centroid of the avalanche is this amount away from the wire

$$\Delta Q^- = \frac{N_e}{U_0}\int E(r)\,\mathrm{d}r = \frac{N_e}{\ln(r_a/r_i)} \ln\frac{r_i}{l_0} \qquad \Delta U^- = \Delta Q^-/C$$

$$\frac{\Delta U^+}{\Delta U^-} = \frac{\ln(r_a/l_0)}{\ln(r_i/l_0)} \qquad r_a \gg r_i \quad \rightarrow \quad \Delta U^+ \gg \Delta U^-$$

in cylindrical geometry, ion signal dominates by typically factor 10 - 100.

Dosimeter for Ionization

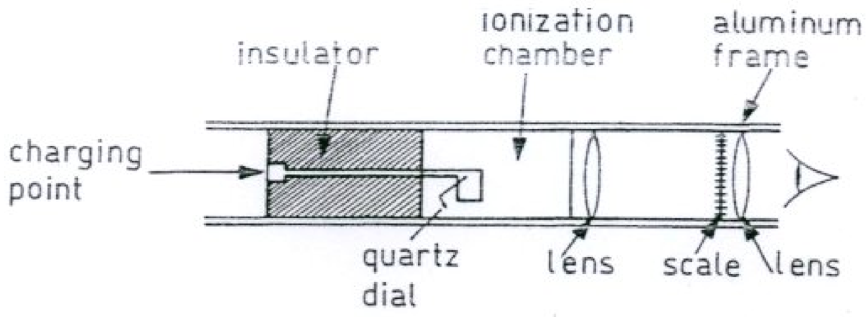

Construction of an ionization pocket dosimeter

- cylindrical capacitor filled with air
- initially charged to potential U_0
- ionization continuously discharges capacitor
- reduction of potential ΔU is measure for integrated absorbed dose (view e.g. via electrometer)

other applications: measure energy deposit of charged particle, should be highly ionizing (low energy) or even stop (then measure total kinetic energy)
nuclear physics experiments with energies of 10 to 100 MeV
combination of ΔE and E measurements $\rightarrow$ particle identification (nuclei)

3.5 Proportional Counter

gas amplification as described above

$$N = A \cdot N_e$$

with a gas gain in vicinity of wire

$$A = \exp \int_{r_k}^{r_i} \alpha(x) \mathrm{d}x$$

charge avalanche typically builds up within 20 μm
effectively it starts at $r_0 = r_i + k\lambda$
k: number of mean free paths needed for avalanche formation
λ: mean free paths of electrons (order μm)

$(2^{10} \cong 1000 \quad 2^{17} \cong 10^5)$

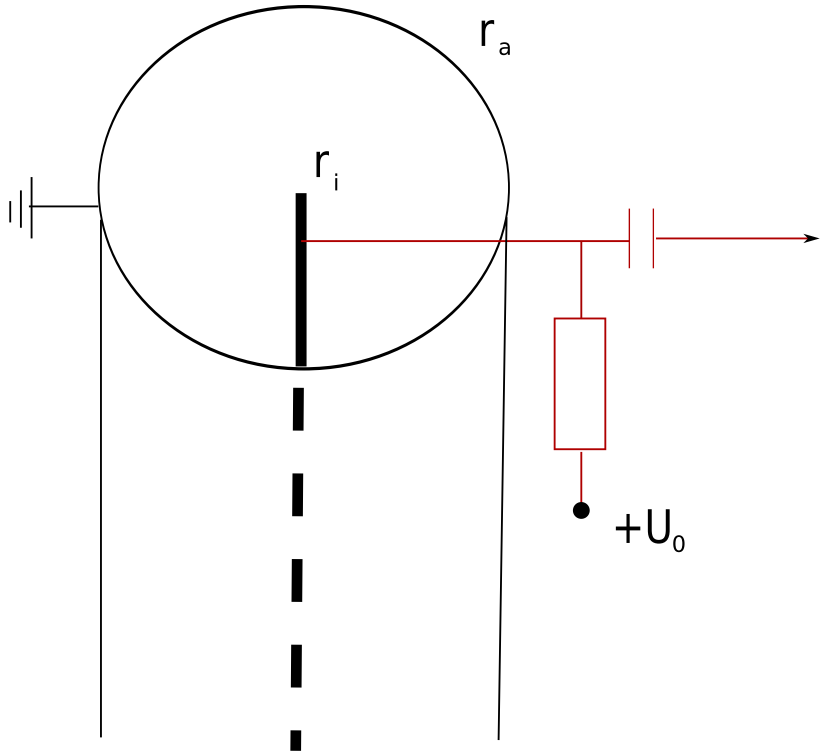

$$\Delta U^- = -\frac{N_e A}{C} \frac{\ln r_0/r_i}{\ln r_a/r_i}$$

$$\Delta U^+ = -\frac{N_e A}{C} \frac{\ln r_a/r_0}{\ln r_a/r_i}$$

$$\frac{\Delta U^+}{\Delta U^-} = \frac{\ln r_a/r_0}{\ln r_0/r_i} = R$$

$r_a = 1$ cm, $r_i = 30\ \mu$m, $k\lambda = 20\ \mu$m for Ar at P_{atm} $\quad \rightarrow R \simeq 10$

In a proportional counter the signal at the anode wire is mostly due to ion drift!

rise time for electron signal as discussed above

$\Delta t^- = \dfrac{\ln(r_a/r_i)}{2\mu^- U_0}(r_0^2 - r_i^2)$ order of ns for $\mu^- = 100 - 1000$ cm^2/Vs
and $U_0 \cong$ several 100 V

ion signal Δt^+ slow, order of 10 ms $\rightarrow$ differentiate with $R_{\text{diff}} \cdot C$

in case $R_{\text{diff}} \cdot C = 1$ ns $\rightarrow$ time structure of individual ionization clusters can be resolved

Typical set-up

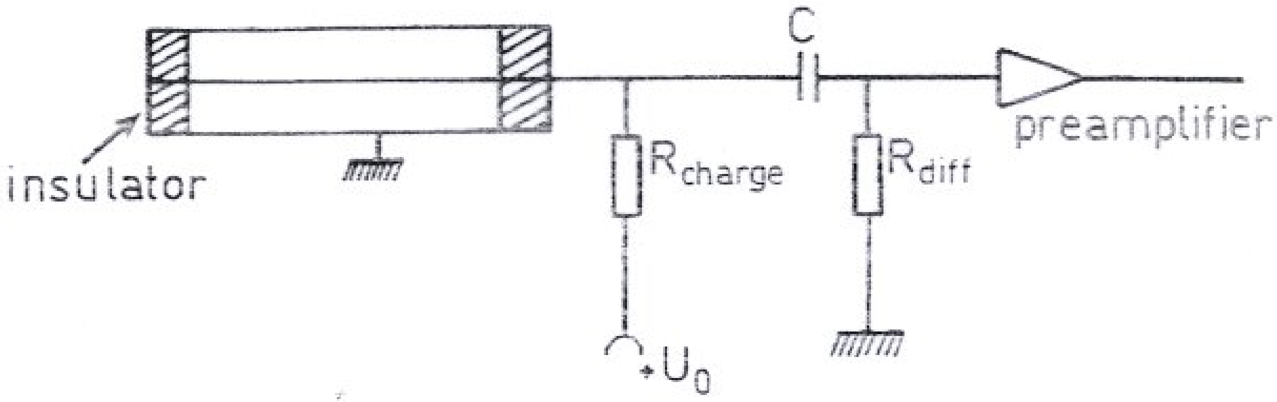

Readout of a proportional counter

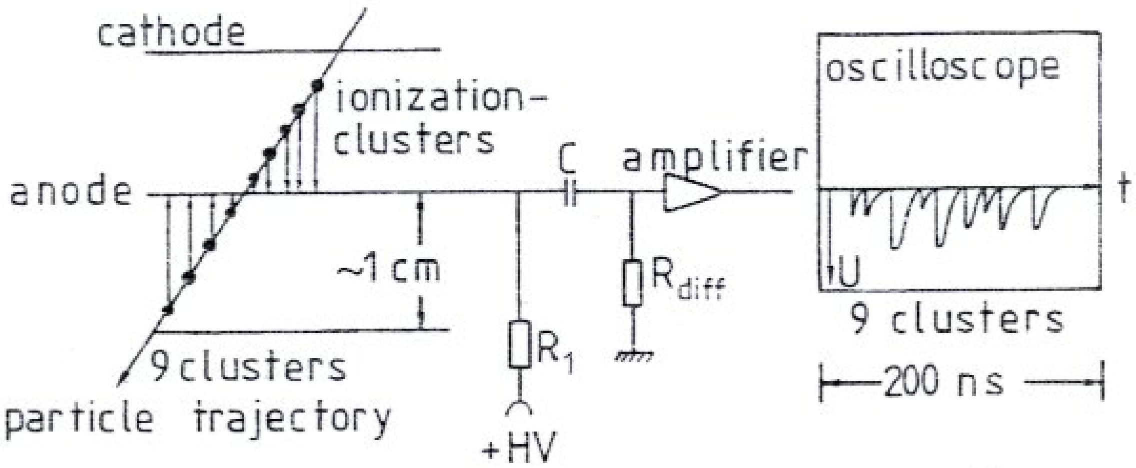

Illustration of the time structure of a signal in the proportional counter

Application outside particle physics: particularly suited to measure X-rays, e.g. 'X-ray imaging' with special electrode geometries for experiments involving synchrotron radiation (high rates!)

Multi-wire proportional chamber

most important application:
Multi-wire proportional chamber MWPC
planar arrangement of proportional counters without separating walls
G. Charpak et al. NIM 62 (1968) 202
Nobel prize 1992, Rev. Mod. Phys. 65 (1993) 591

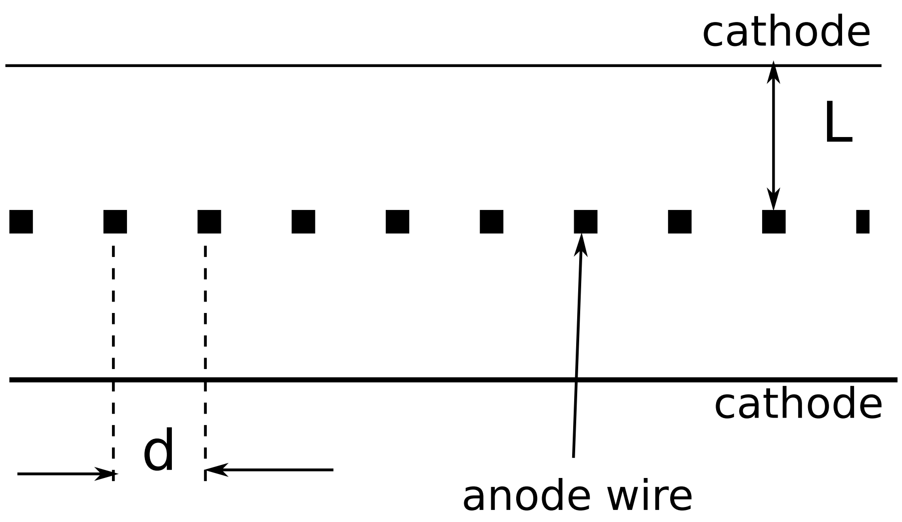

allows: tracking of charged particles, some PID capabilities via $\mathrm{d}E/\mathrm{d}x$
large area coverage, high rate capability

as compared to cylindrical arrangement field geometry somewhat different

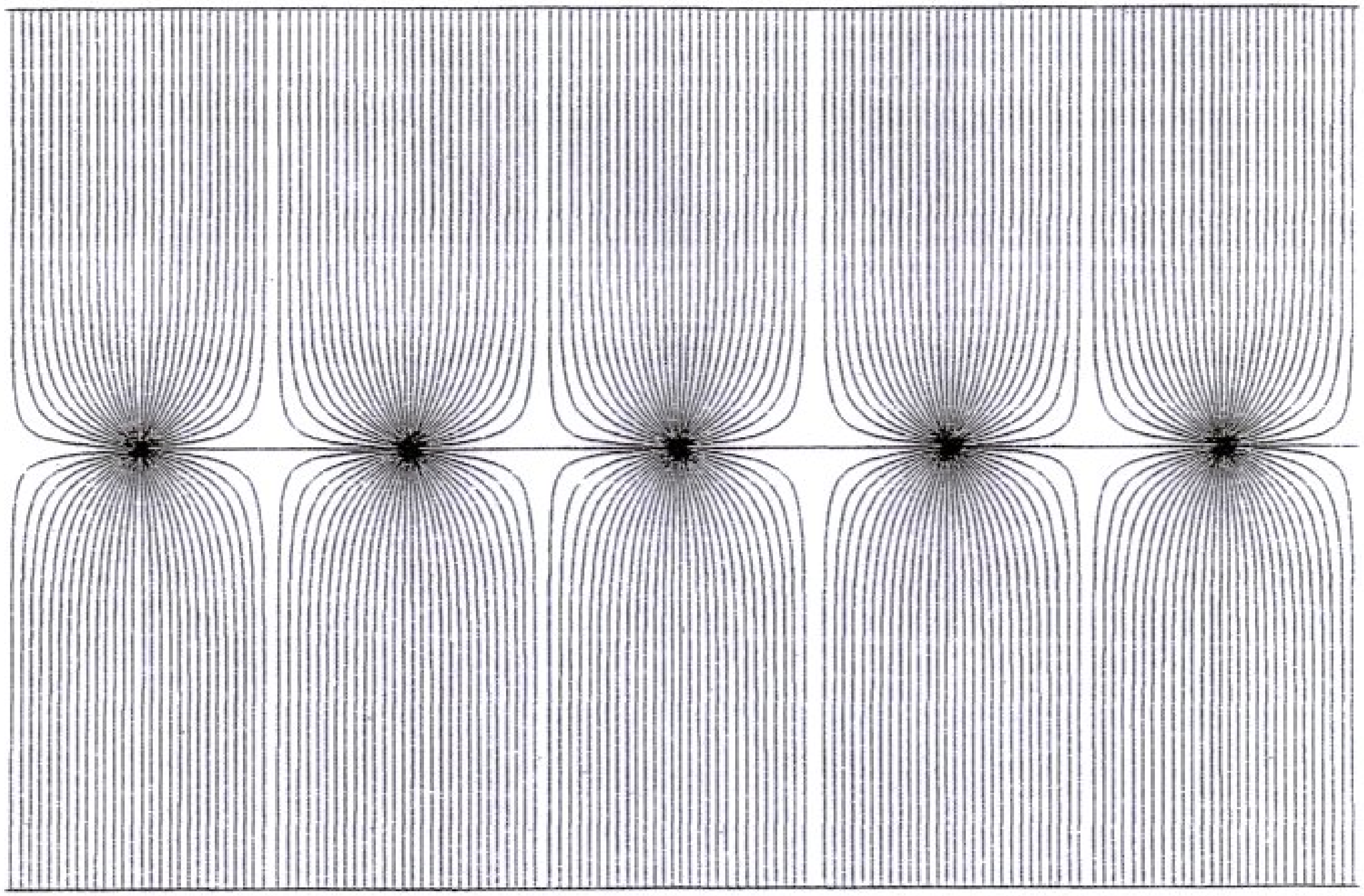

typical parameters:

$d = 2 - 4$ mm

$r_i = 15 - 25$ μm

$L = 3 - 6$ mm

$U_0 =$ several kV

total area: many m^2

typical geometry of electric field lines in multi-wire proportional chamber

in vicinity of anode wire: radial field
far away homogeneous (parallel-plate capacitor)

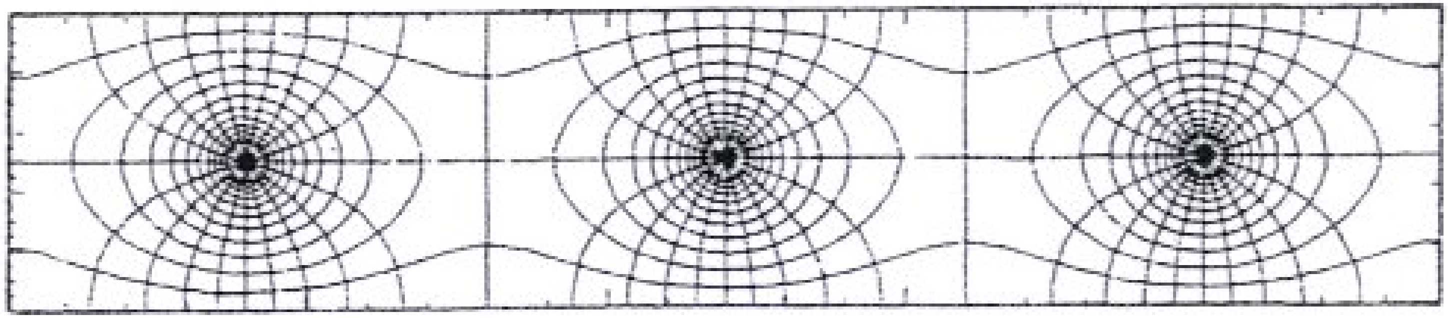

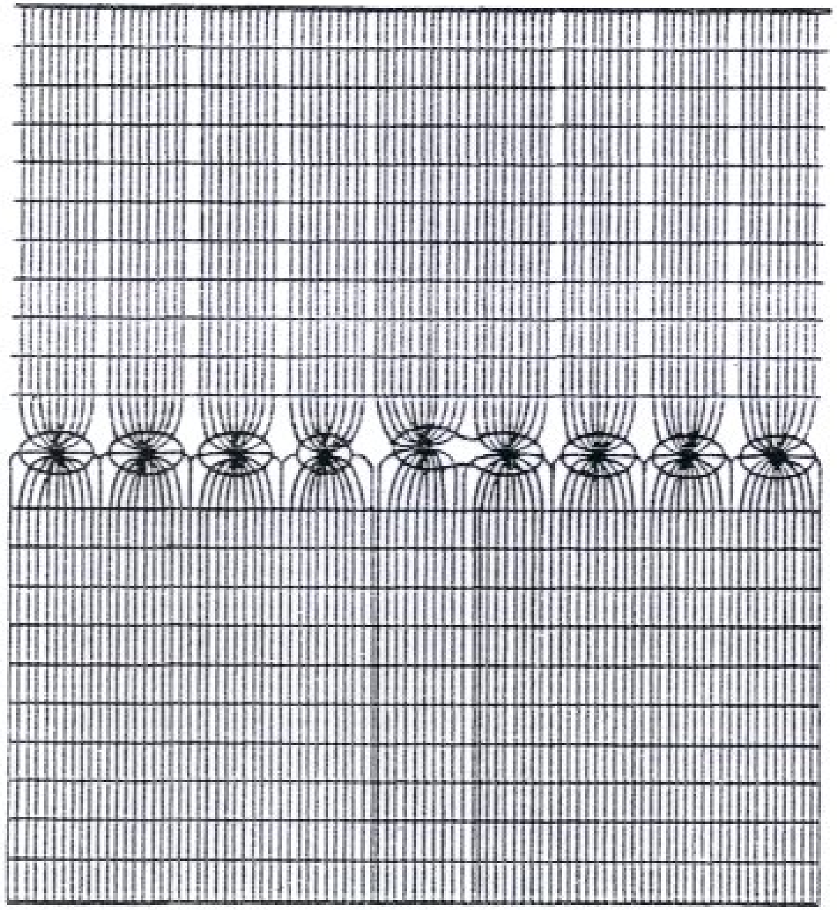

Field lines and equipotential lines

Difficulty:
even small geometric displacement of an individual wire will lead to effect on field quality.

need of high mechanical precision, both for geometry and wire tension (electrostatic effects and gravitational wire sag, see below)

- electrons from primary and secondary ionization drift to closest anode wire
- in vicinity of wire gas amplification $\rightarrow$ formation of avalanche
  ends when electrons reach wire or when space charge of positive ions screens electric field below critical value
- signal generation due to electron- and (mostly) slow ion-drift

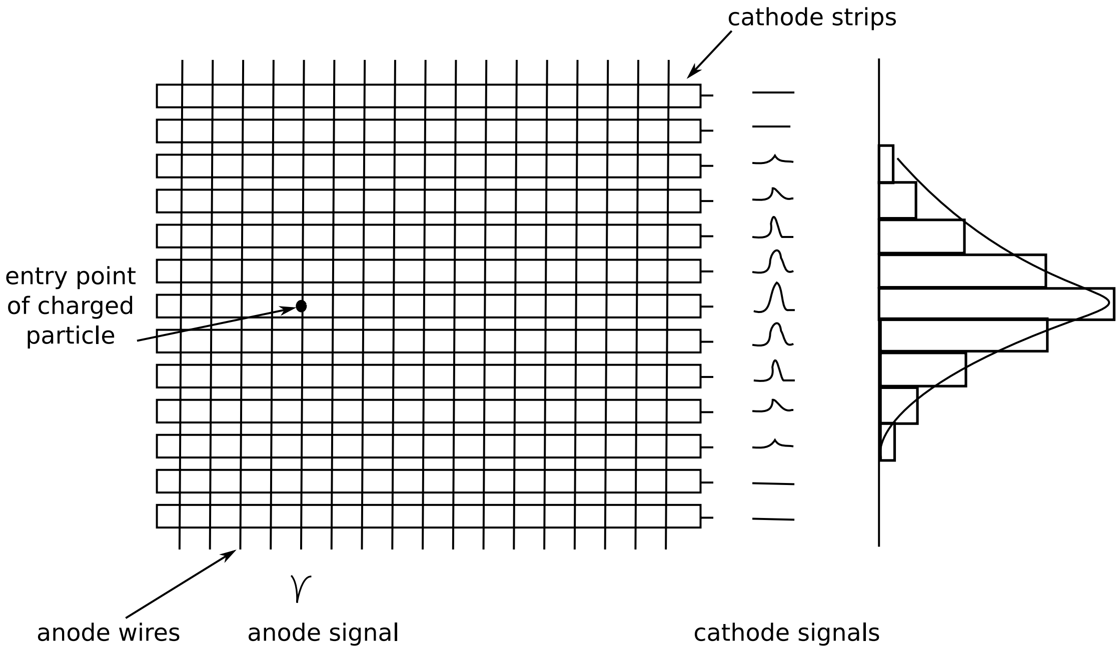

typical space point resolution:
since only information about closest wire $\rightarrow$
$\delta_x = d/\sqrt{12} = 577\ \mu\text{m}$ for $d = 2$ mm

not very precise and only 1-dimensional

can be improved by segmenting cathode and reading out of signal induced on cathode spread-out over more than 1 strip

the center of gravity of signals on cathode strips can be determined with precision of $50 \ldots 300\ \mu\text{m}$! use charge sharing between adjacent strips

Note: The dimension with good resolution is along the wire, perpendicular always $d/\sqrt{12}$.

Resolving ambiguities in case of 2 or more hits in one event:
different orientation of segmentation in several cathode planes

two particles traversing MWPC: with only one orientation of segmentation (strips) possibilities ●● and ○○ cannot be distinguished and one obtains 4 possible coordinates for tracks: 2 real and 2 'ghosts', resolved by second induced strip pattern

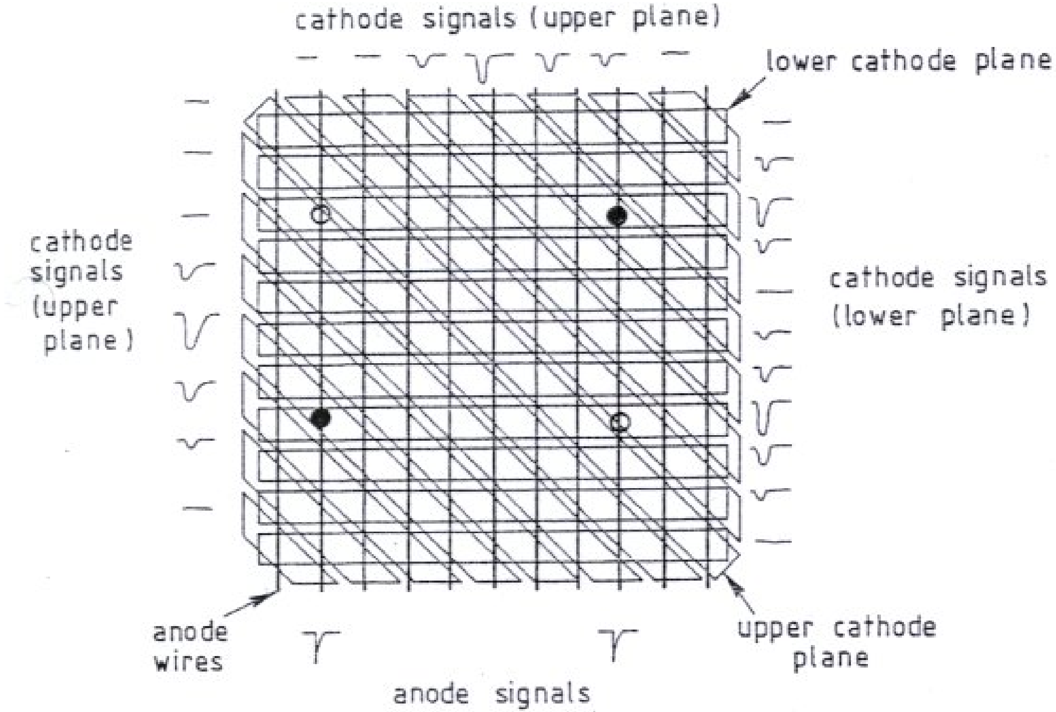

Illustration of the resolution of ambiguities for two particles registered in a multi-wire proportional chamber

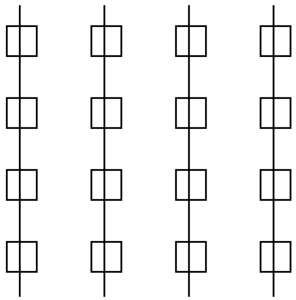

for high hit density environment segmentation of cathode into pads truly 2-d measurement.
but: number of read-out channels grows quadratically with area ($$)

Stability of wire geometry I

Can we make resolution better and better by putting wires closer and closer?
practical difficulty in stringing wires precisely closer than 1 mm
fundamental limitations: stability of wire geometry

- electrostatic repulsion between anode wires, in particular for long wires
  $\rightarrow$ can lead to 'staggering'
  to avoid this, the wire tension T has to be larger than a critical value T_0 given by

$$U_0 \leq \frac{d}{lC}\sqrt{4\pi\epsilon_0 T_0}$$

with

wire length l
wire distance d
capacity per unit length for cylinder $C = \dfrac{4\pi\epsilon_0}{2\ln\left(r_a/r_i\right)}$

approximation for MWPC with distance anode-cathode $L \gg d \gg r_i$

$$C = \frac{4\pi\epsilon_0}{2\left(\frac{\pi L}{d} - \ln\frac{2\pi r_i}{d}\right)}$$

leading to

$$T_0 \geq \left(\frac{U_0 l}{d}\right)^2 4\pi\epsilon_0 \left[\frac{1}{2\left(\frac{\pi L}{d} - \ln\frac{2\pi r_i}{d}\right)}\right]^2$$

with $l = 1$ m, $U_0 = 5$ kV, $L = 10$ mm, $d = 2$ mm, $r_i = 15\ \mu$m $\rightarrow T_0 = 0.49$ N ($\simeq 50$ g)

Stability of wire geometry II

- for horizontal wires also gravity $\rightarrow$ sag

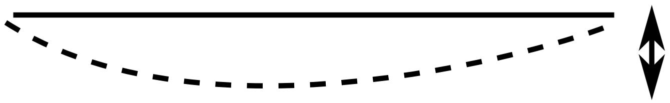

$$f = \frac{\pi r_i^2}{8} \rho g \frac{l^2}{T} = \frac{mlg}{8T}$$

gold-plated W-wire $r_i = 15\ \mu$m, T as above $\rightarrow f = 34\ \mu$m $\rightarrow$ visible difference in gain

some of these problems avoided by 'straw tube chambers' (assembly of single-wire proportional counters):

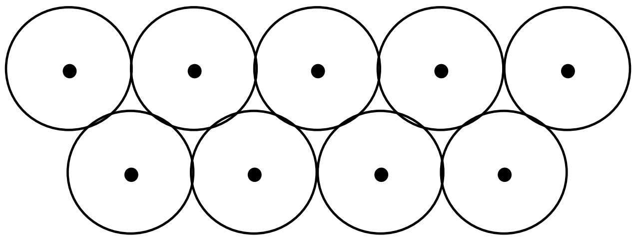

cylindrical wall = cathode
aluminized mylar foil
introduced in 1990ies

further big (!) advantage: a broken wire affects only 1 cell, not entire chamber
straw diameter: $5 - 10$ mm, can be operated at over-pressure,
space point resolution down to 160 μm (e.g. LHCb Outer Tracker)
short drift lengths: enable high rates
operation in magnetic field without degradation of resolution
concept employed in several LHC detectors

- can wires be avoided entirely?

ease of construction
stability
. . .
anode can actually be realized by microstructures on dielectrics

example: microstrip gas detector (developed in 1990ies)

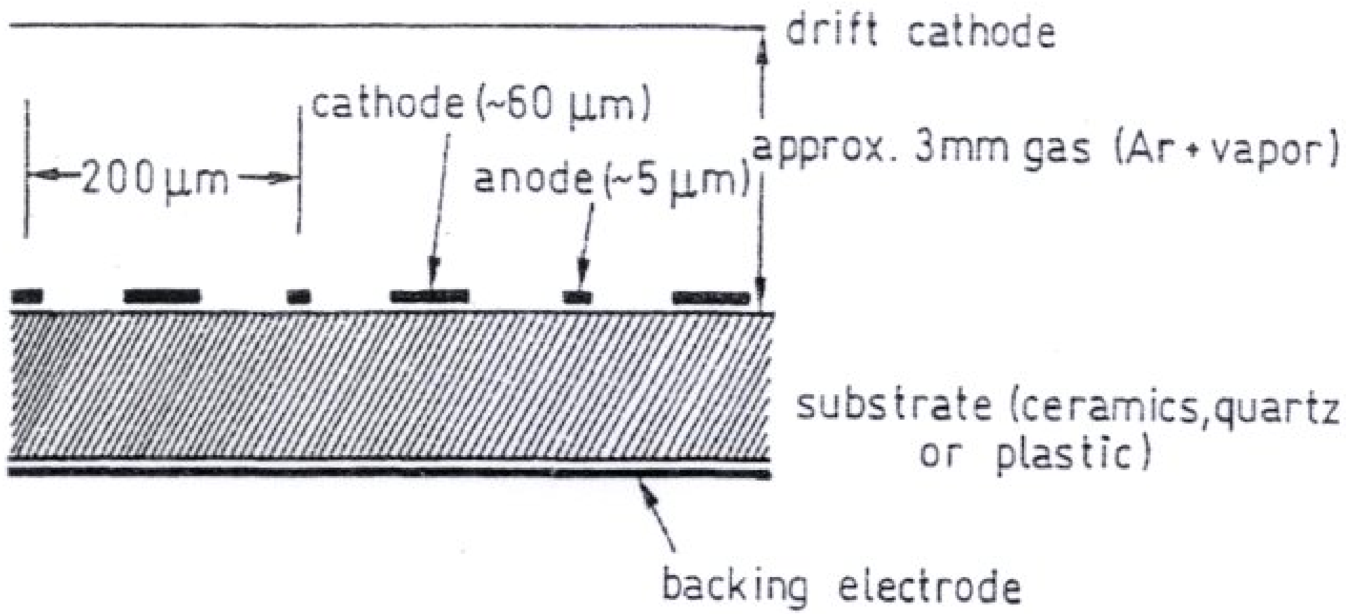

Schematic arrangement of a microstrip gas detector schematics of a **microstrip gas chamber**

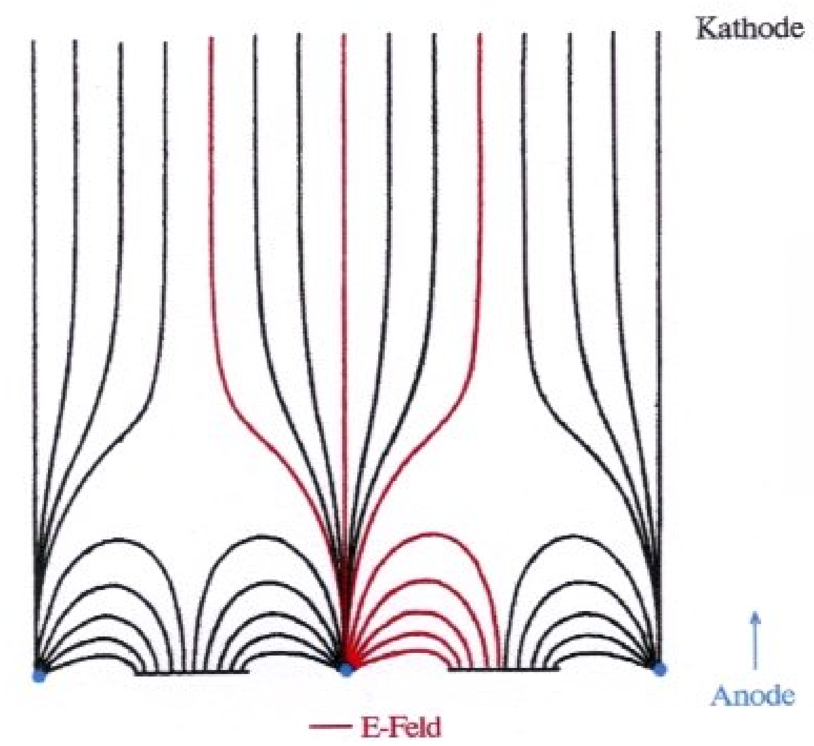

directly above anode strip high density of field lines

advantages

- ions drift only 100 μm
- high rate capability without build-up of space charge
- resolution

fine structures can be fabricated by electron lithography on ceramics, glass or plastic foil on which a metal film was previously evaporated.

problems

charging of isolation structure

$\rightarrow$ time-dependence of gas gain

$\rightarrow$ sparks, destruction of anode structure, corrosion of insulator

basically not a succeessful concept - lifetime of detector too limited

Gas electron multiplier

a possible solution:
pre-amplification with GEM foil

GEM: gas electron multiplier
invented by F. Sauli (CERN) ($\sim$1997)

allows reduced electric field
in vicinity of anode structures.

but: ease of construction again partly eliminated and danger of discharge on foil (huge capacitance)

upgrade of Alice TPC for 50 kHz PbPb collisions based on quadruple GEM layers
challenge: to keep ion feedback below 1 %

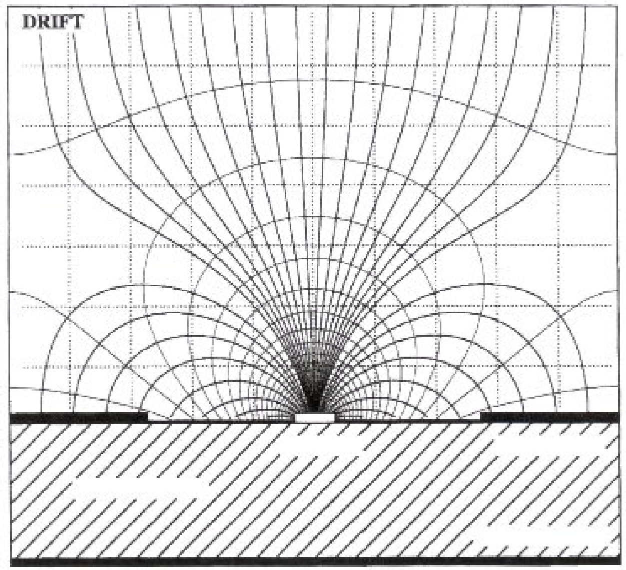

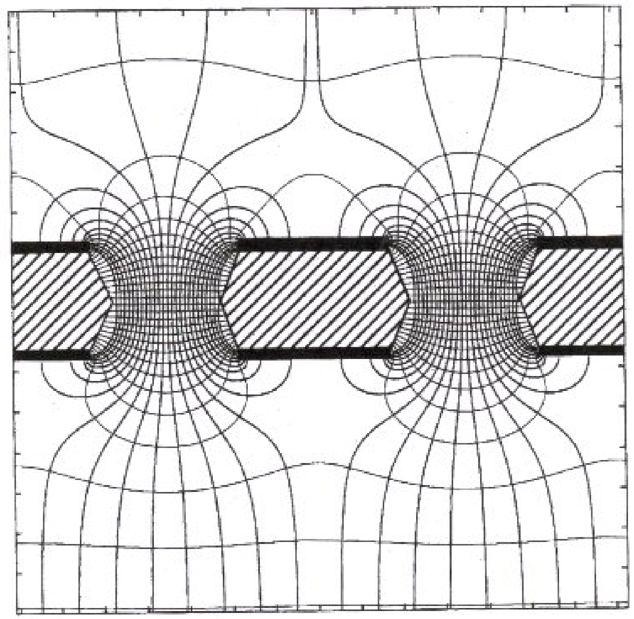

3.6 Drift chambers

invented by A. Walenta, J. Heintze in 1970 at Phys. Inst. U.Heidelberg (NIM 92 (1971) 373)

Principle

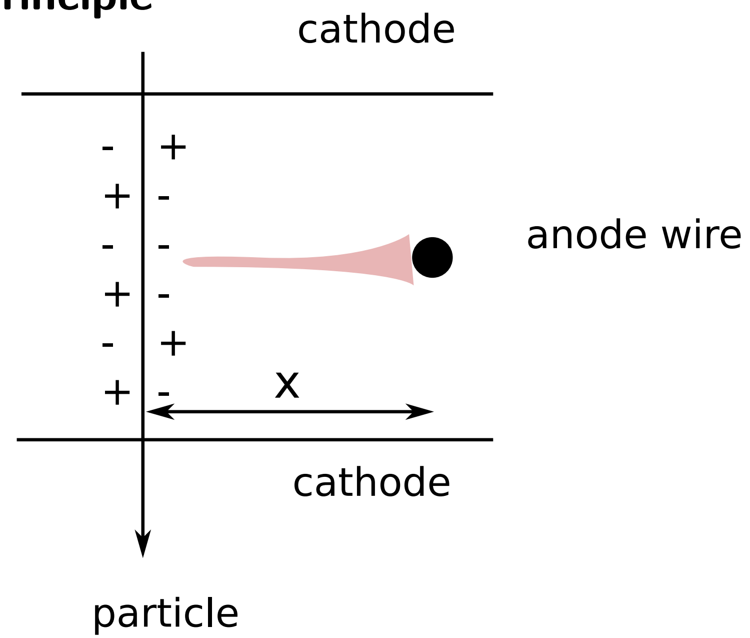

time measurement:

$$x = v_D^- \cdot \Delta t$$

v_D^-: drift velocity of electrons

or, in case drift velocity changes along path

$$x = \int v_D^-(t)\mathrm{d}t$$

needs well defined drift field $\rightarrow$ introduce additional field wires in between anode wires.
but: In that case number of anode wires can be reduced in comparison to MWPC at improved spatial resolution

$$\left.\begin{array}{l} v_D^- \simeq 5 \text{ cm}/\mu\text{s} \\ \text{time resolution of front end electronics } \sigma_t \simeq 1 \text{ ns} \end{array}\right\} \quad \sigma_x \simeq 50\ \mu\text{m is possible}$$

but the resolution is affected by diffusion of drifting electrons and statistical fluctuations in primary ionization (in particular in vicinity of wire).

factors affecting spatial resolution in a drift chamber:

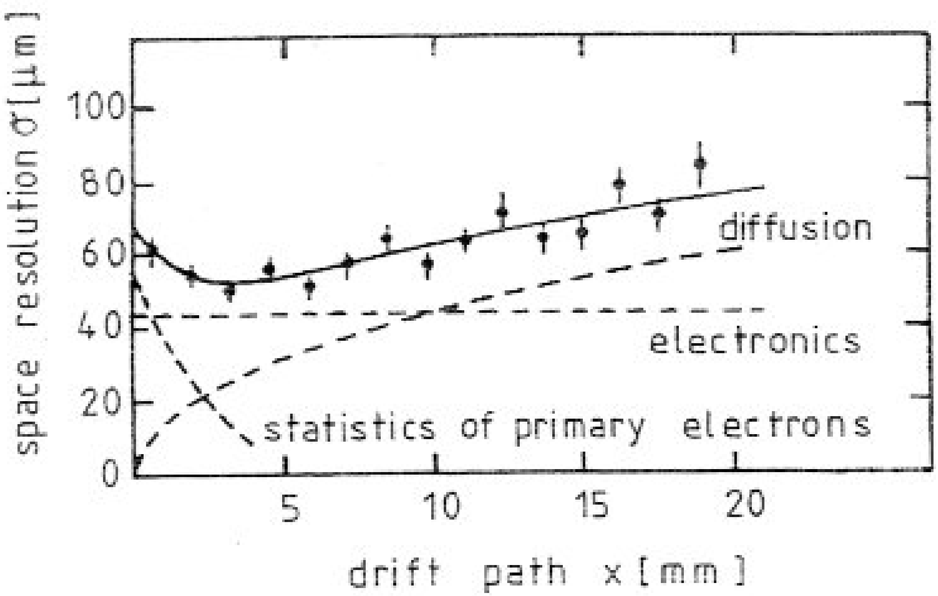

spatial resolution in a drift chamber as a function of the drift path

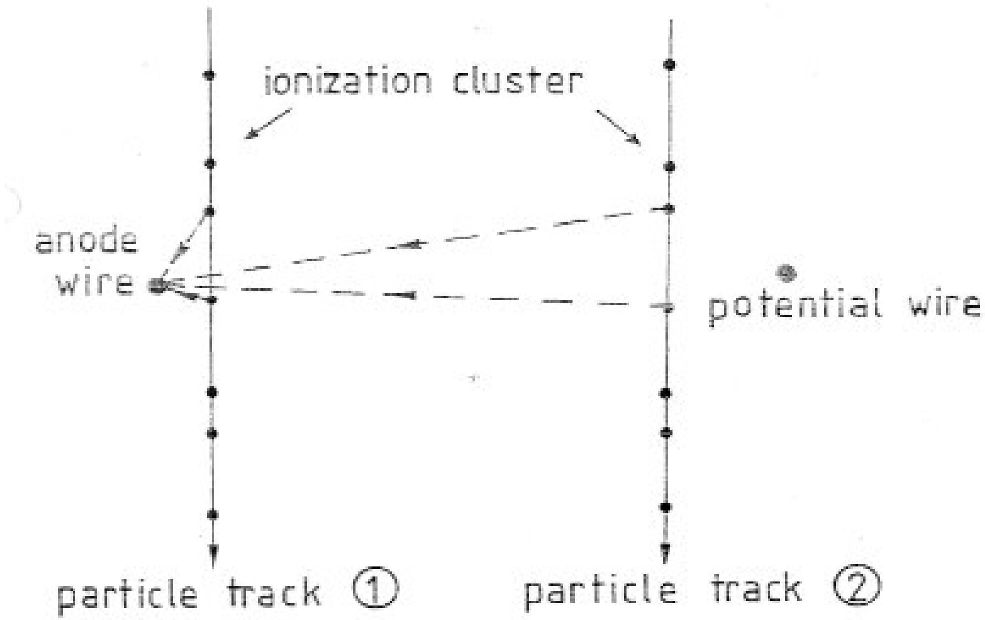

illustration of different drift paths for 'near' and 'distant' particle tracks to explain the dependence of the spatial resolution on the primary ionization statistics

Difficulty: time measurement cannot distinguish between particle passing to the left or to the right of the anode wire → 'left-right ambiguity'

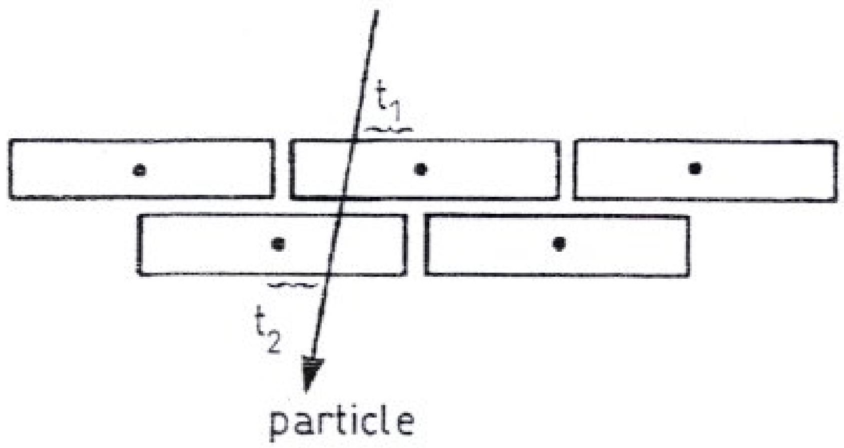

resolution of the left-right ambiguity in a drift chamber

need 2 layers displaced relative to each other by half the wire distance: 'staggered wires'

How to achieve field quality good enough for drift chamber?

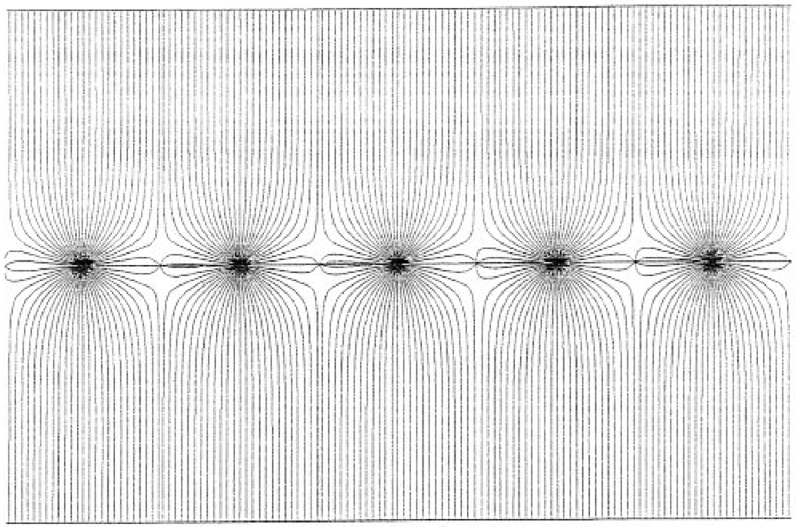

in a MWPC in between anode wires there are regions of very low electric field (see above)

the introduction of additional **'field wires'** at negative potential relative to anode wires strongly improves the field quality

essential for drift chamber where spatial resolution is determined by drift time variations and not by segmented electrode structure

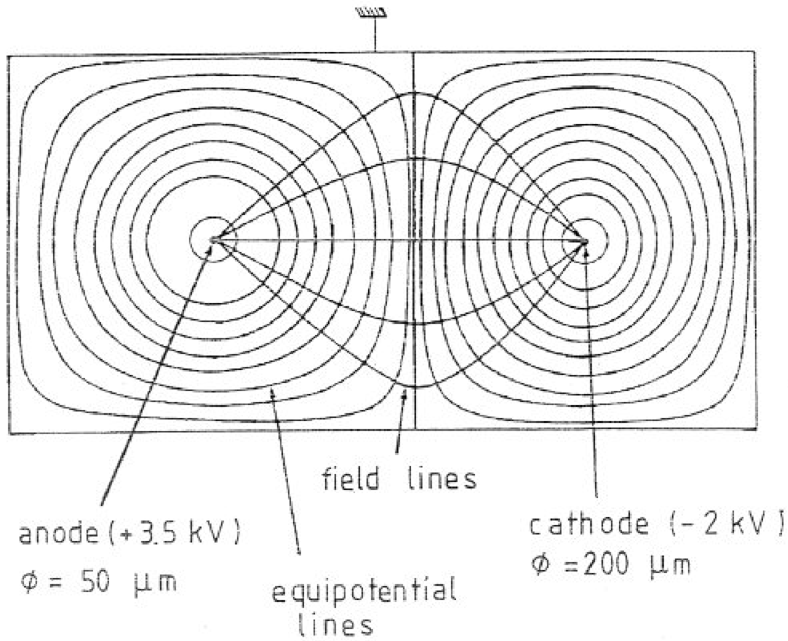

one can build **very large** drift chambers; in this case one introduces a voltage divider by cathode strips connected via resistors, very few or even only one wire.

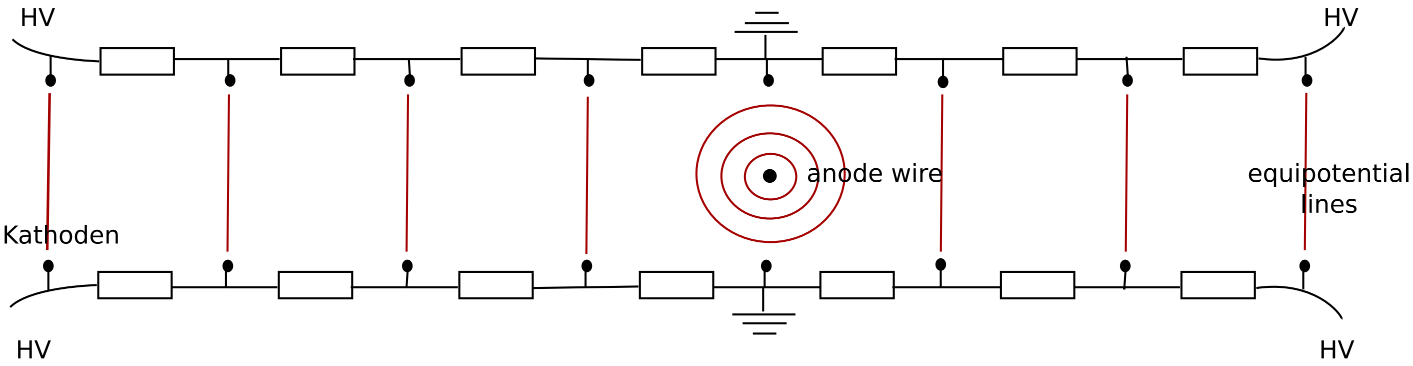

space point resolution limited by mechanical tolerance

for very large chambers
 $(100 \times 100\ cm^2)$ $\simeq 200\ \mu m$

for very small chambers
 $(10 \times 10\ cm^2)$ even $\simeq 20\ \mu m$

but: hit density has to be low!

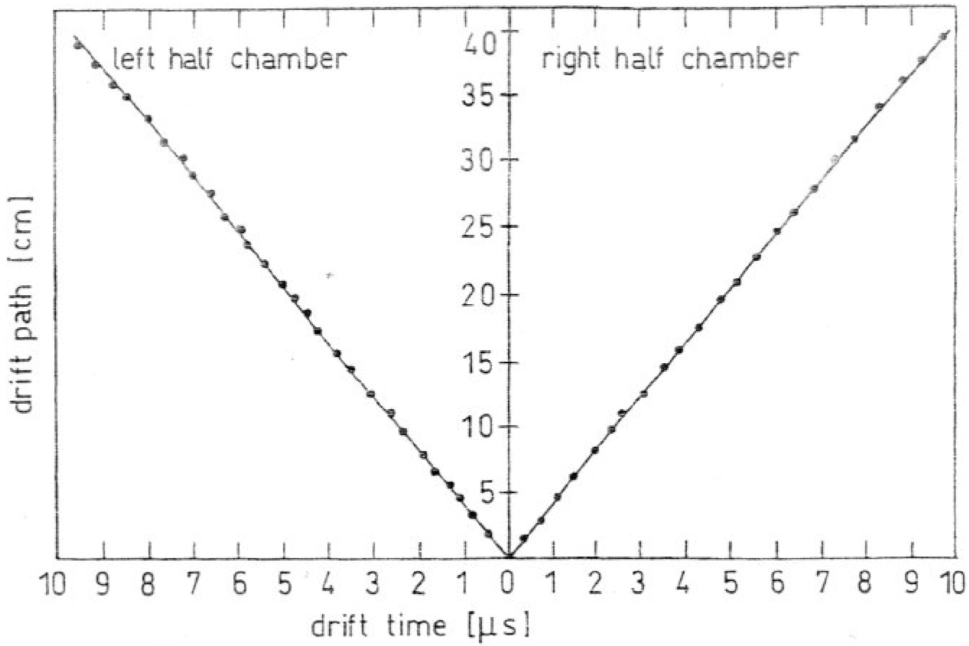

drift time - space relation in a large drift chamber $(80 \times 80\ cm^2)$ with only one anode wire (Ar + iso-butane 93/7)

field can even be formed by charging up of insulating chamber wall with ions
after some charging time ions cover insulating layer, no field line end there

Resistive plate counter:

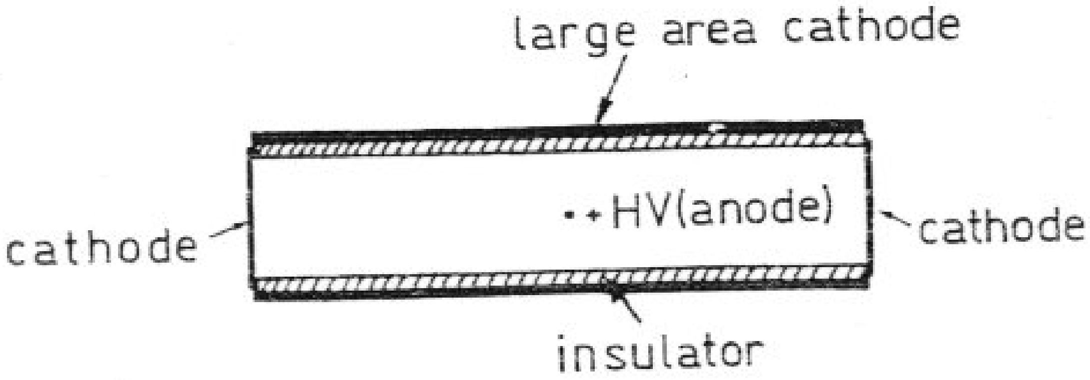

Principle of construction of an electrodeless drift chamber

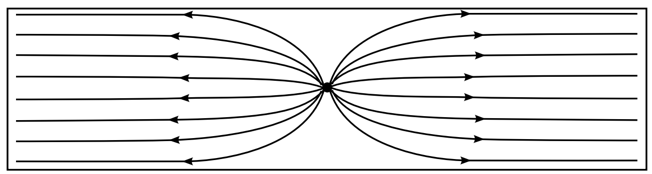

After charging the insulating layer with ions

3.7 Cylindrical wire chambers

in particular for experiments at storage rings (colliders) to cover maximum solid angle

- initially multi-gap spark chambers, MWPC's
- later cylindrical drift chambers, jet chambers
- today time projection chambers (TPC)

generally these cylindrical chambers are operated in a magnetic field $\rightarrow$ measurement of radius of curvature of a track $\rightarrow$ momentum (internally within one detector)

$$p\ (\mathrm{GeV/c}) = 0.3 \cdot B\ (\mathrm{T}) \cdot \rho\ (\mathrm{m})$$

Principle of a cylindrical drift chamber I

principle of a cylindrical drift chamber: wires in axial direction (parallel to colliding beams **and** magnetic field)

alternating anode and field wires

- one field wire between 2 anode wires
- cylindrical layers of field wires between layers of anode wires → nice drift cells

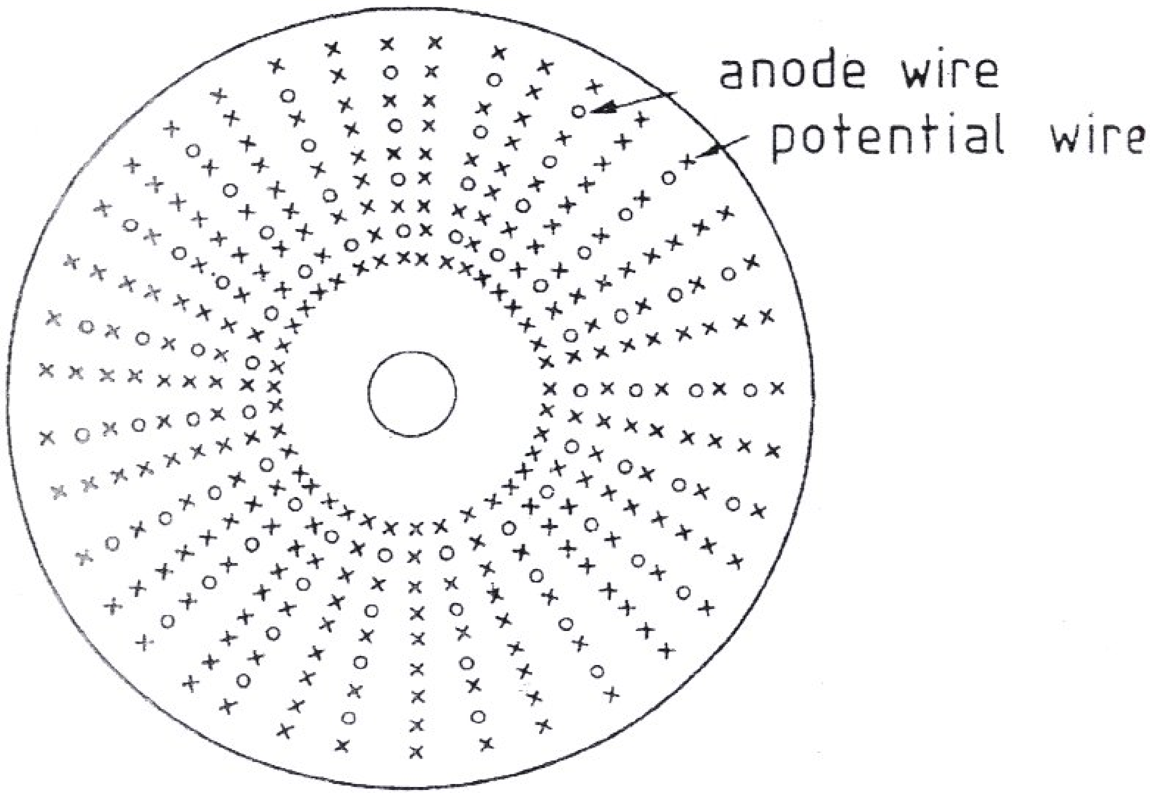

Principle of a cylindrical drift chamber II

different drift cell geometries:

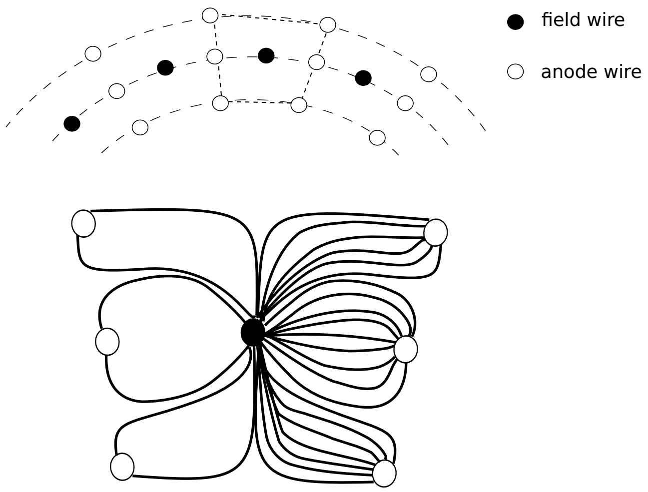

open drift cell

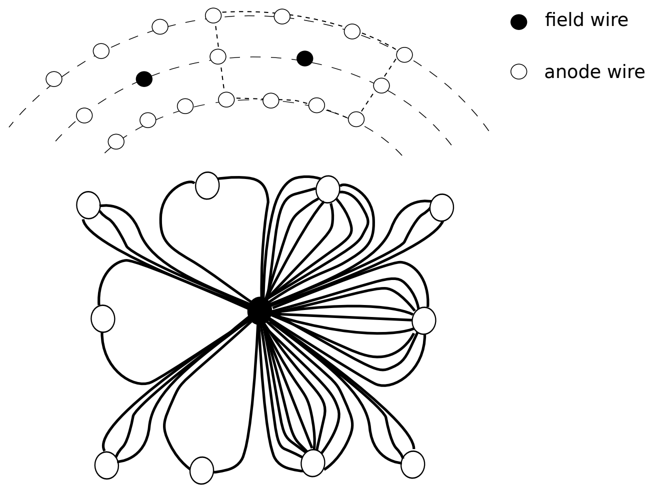

closed drift cell

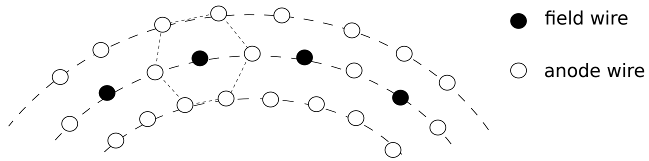

also hexagonal drift cell

always thin anode wires ($\varnothing \simeq 30\ \mu$m) and thicker field wires ($\varnothing \simeq 100\ \mu$m), generally field quality better for more wires per drift cell, but:

- more labor-intensive construction
- wire tension enormous stress on end plates, e.g. for chamber with 5000 anode and 15000 field wires $\rightarrow$ 2.5 t on each endplate

Determination of coordinate along the wire

- current measurement on both ends of anode wire
  charge division, precision about 1% of wire length

$$z \propto \frac{I_1 - I_2}{I_1 + I_2}$$

- time measurement on both ends of wire
- 'stereo wires': layer of anode wires inclined by small angle γ ('stereo angle')
  $\rightarrow \sigma_z = \sigma_x / \sin\gamma$

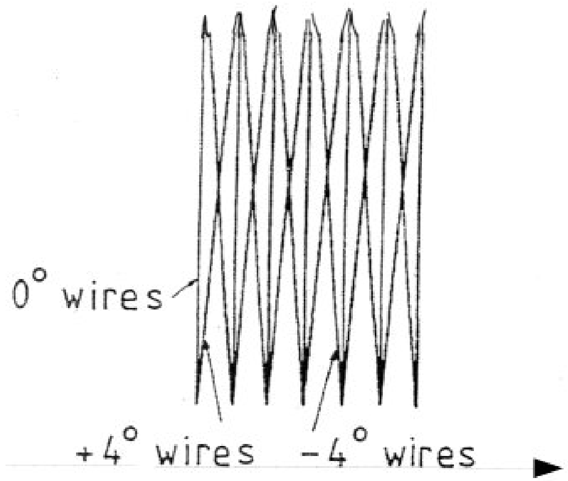

illustration of the determination of the coordinate along the anode stereo wires in general drift field E perpendicular to magnetic field $B \rightarrow$ Lorentz angle for drifting charges

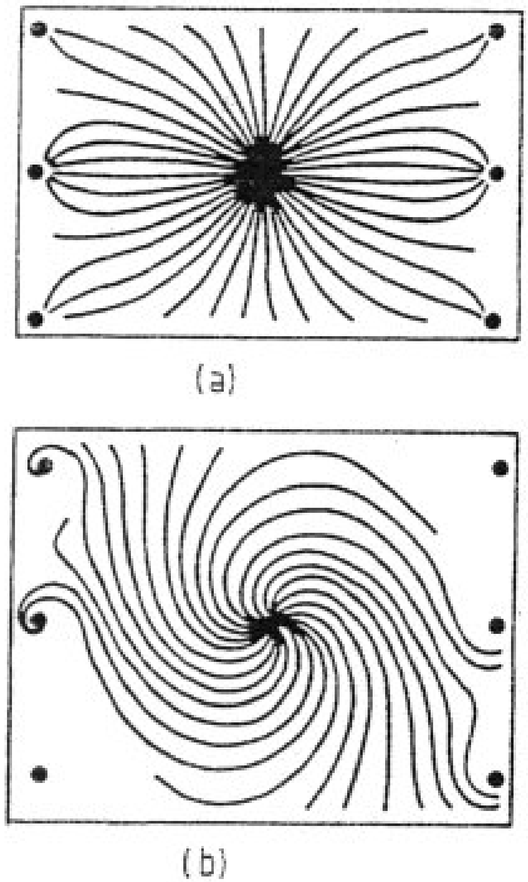

drift trajectories in an open rectangular drift cell a) without and b) with magnetic field

3.8 Jet drift chambers

large drift cells

optimize number of measurements per track

(typically 1/cm)

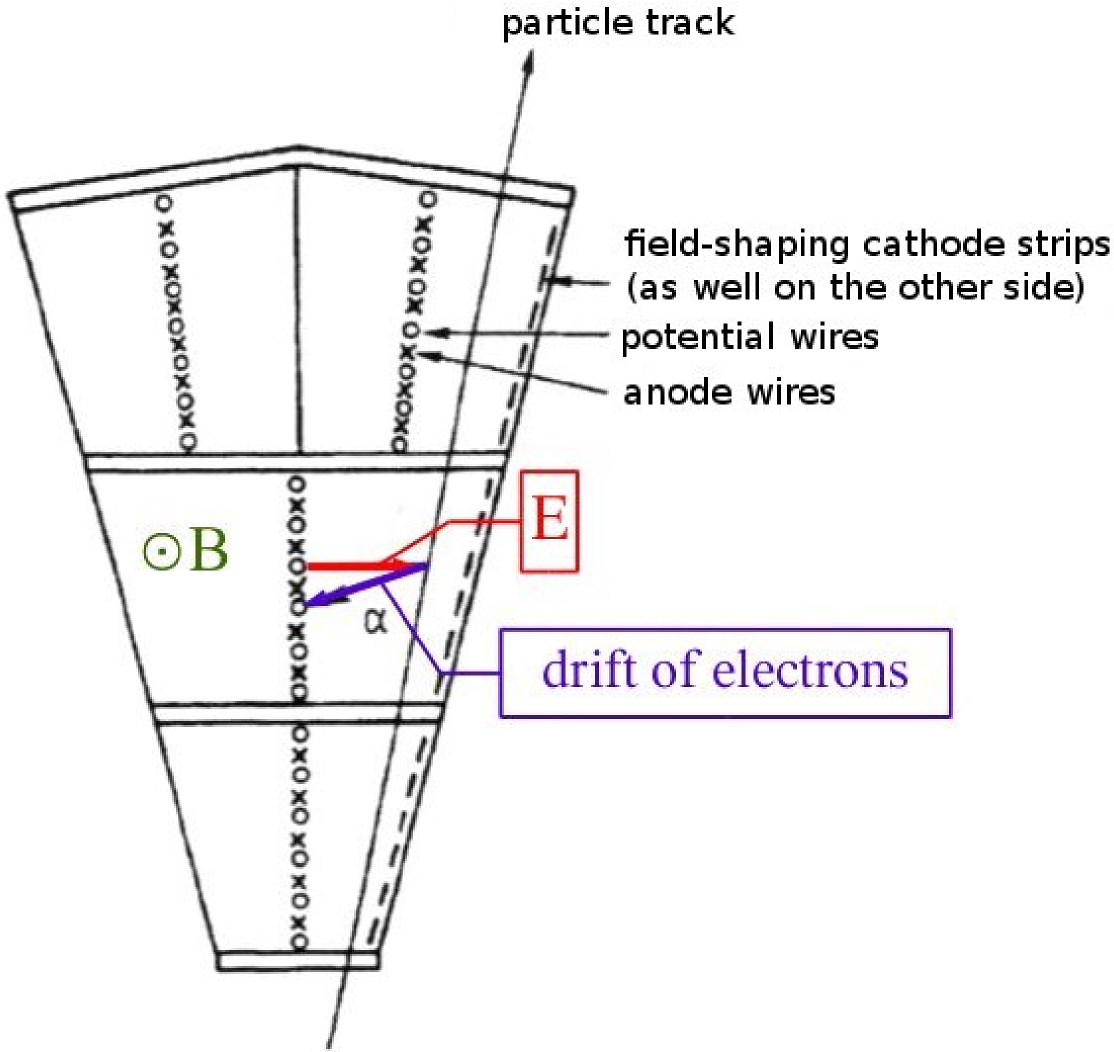

example: JADE jet chamber for PETRA, built by J.Heintze et al. Phys. Inst. U. Heidelberg
length: 2.34 m, radial track length: 57 cm, 47 measurements per track
$\sigma_{r\phi} = 180\ \mu$m, $\sigma_z = 16$ mm

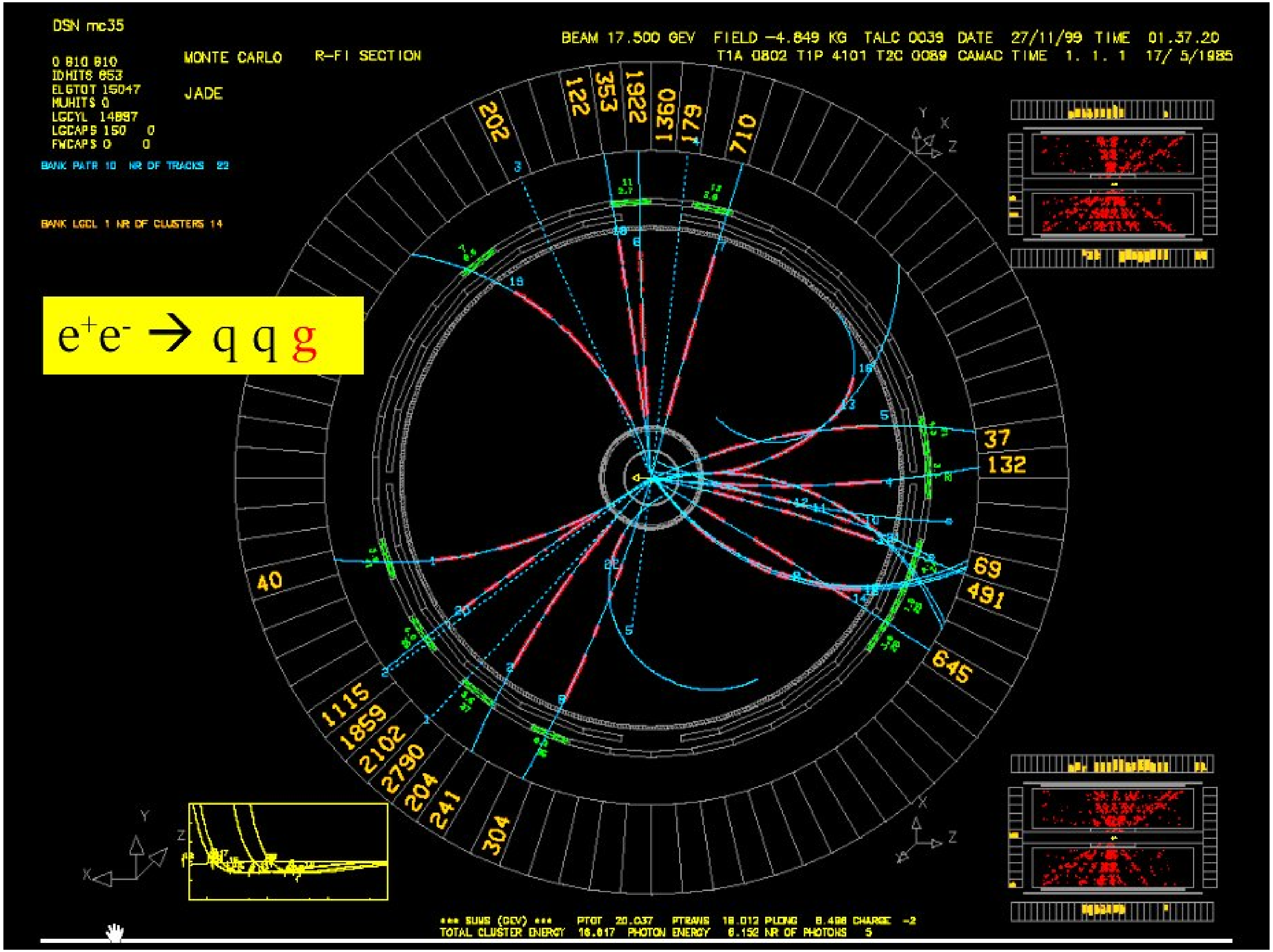

3-jet event by JADE – measurements taken at PETRA → discovery of gluon

another example: OPAL at CERN LEP: central tracking chamber built by team from Phys. Inst. Heidelberg – Heintze, Wagner, Heuer, ...
length: 4 m, radius: 1.85 m, 159 measurements per track, gas: $Ar/CH_4/C_4H_{10}$ at 4 bar
$\sigma_{r\phi} = 135\ \mu$m, $\sigma_z = 60$ mm

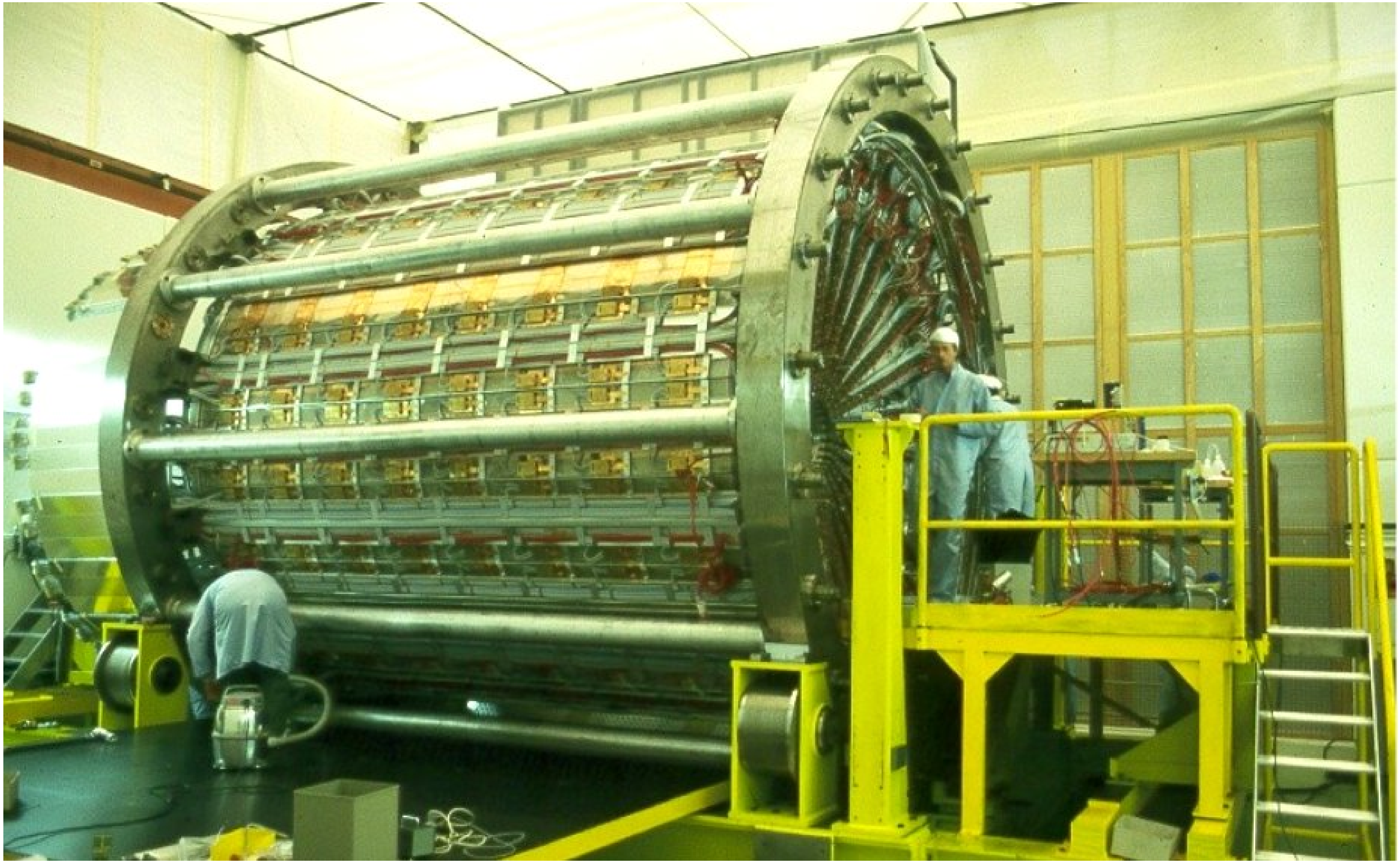

interior of jet chamber of OPAL

application for heavy ion collisions: FOPI (experiment at SIS at GSI):
central drift chamber (CDC), D. Pelte and N. Herrmann Phys. Inst. U.Heidelberg

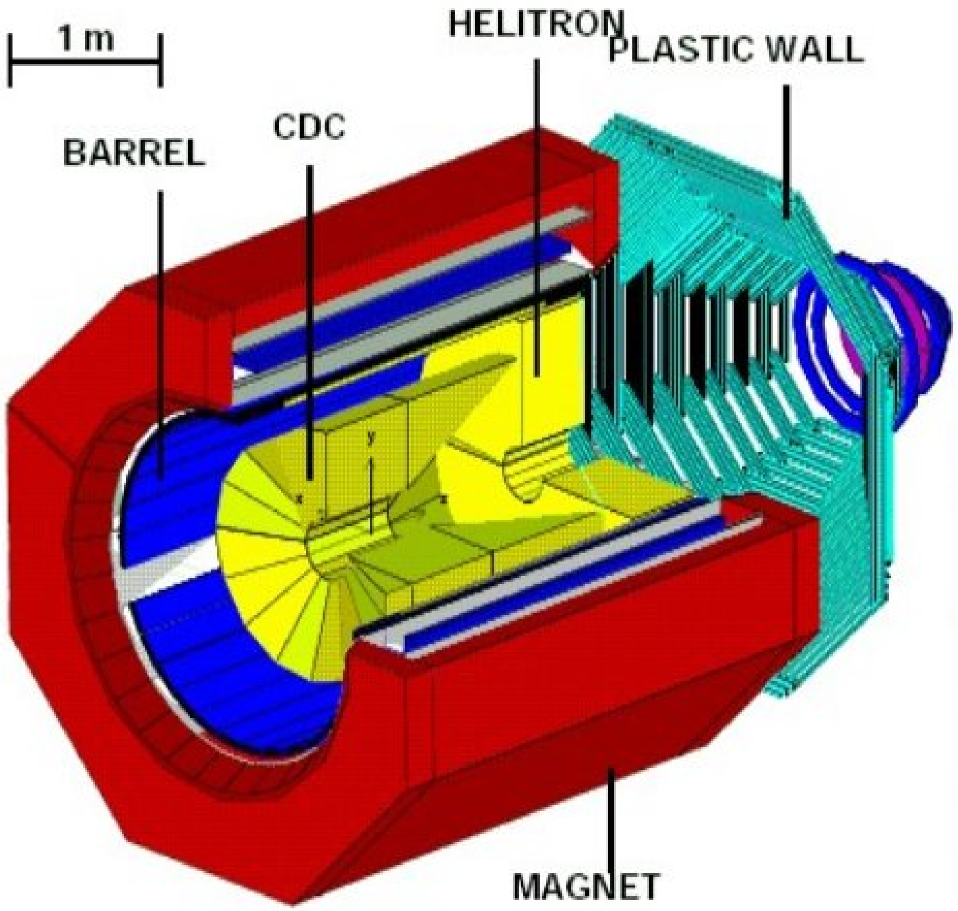

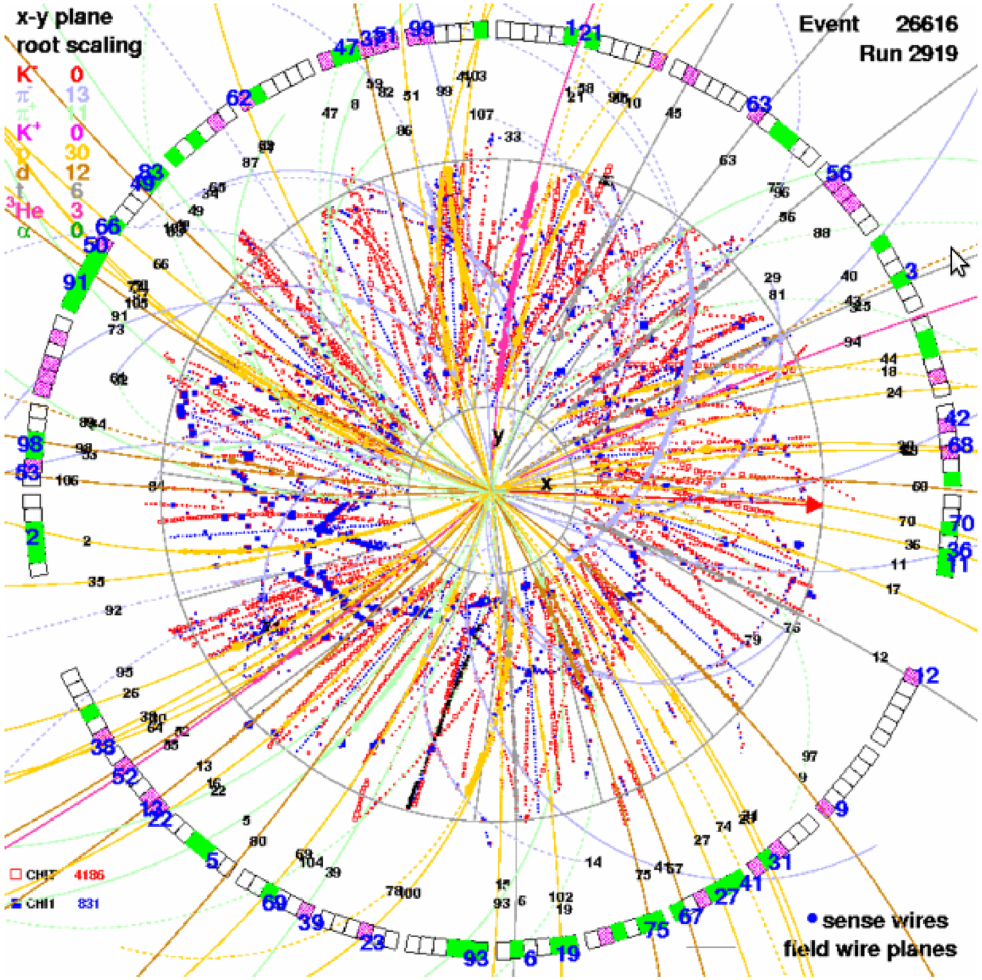

3.9 Time Projection Chamber TPC

3-dimensional measurement of a track – ‘electronic bubble chamber’
invented by D. Nygren in 1974 at Berkeley

(mostly) cylindrical detector
central HV cathode
MWPCs at the endcaps of the cylinder
electrons drift in homogenous electric fields towards MWPC, where arrival time and point and amount of charge are continuously sampled (flash ADC)
generally with $B \parallel E \rightarrow$ Lorentz angle $= 0$

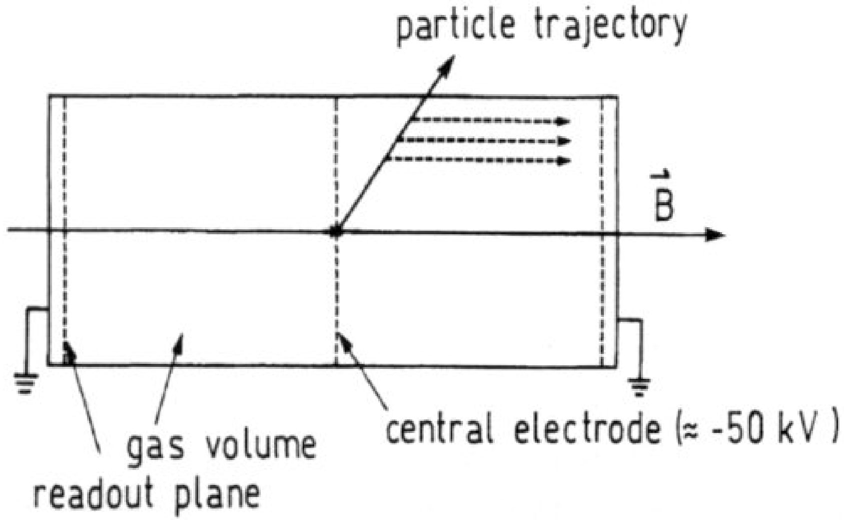

Working principle of a TPC

advantages:

- complete track determination within one detector $\rightarrow$ good momentum measurement
- relatively few wires (mechanical advantage)
- since also charge is measured: particle identification via $\mathrm{d}E/\mathrm{d}x$
- drift parallel to $B \rightarrow$ transverse diffusion suppressed by factors $10 - 100$ (see above)

disadvantages

- drift time: relatively long - tens of microseconds $\rightarrow$ not a high rate detector
- large data volume

principle of operation of a TPC

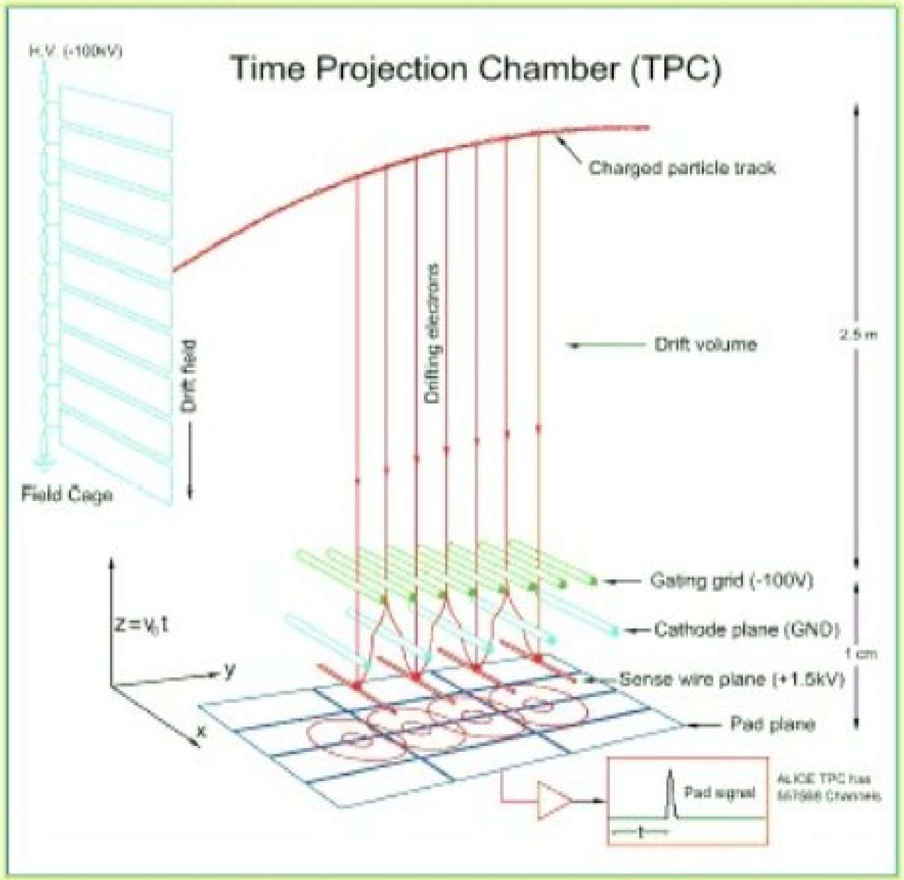

continuously sample induced charge or current signals in a MWPC at end of long drift path

z-dim given by drift time
x-dim given by charge sharing of cathode pads
y-dim given by wire/pad number

truly 3-dimensional measurement of ionization points of entire track and in fact of many tracks simultaneously

typical resolution:
z: mm
$r\phi$ or x: 150–300 μm
y: mm
dE/dx: $5 - 10\%$, trick:
kill Landau tail by evaluating truncated mean

challenges:

- long drift path (attachment, diffusion, baseline)
- large volume (precision)
- large voltages (discharges)
- extreme load in Pb+Pb collisions
  space charge in drift volume
  leads to distortion of $\vec{E}$
  gating grid opened (fast ~ 1 μs) for triggered events only, otherwise opaque ($\pm\Delta V$)

serious difficulty:
space charge effects since also ions have long drift path and move factor 1000 more slowly, positive ions change effective E-field in drift region, most (5000:1) come from amplification region

trick: invention of gating grid

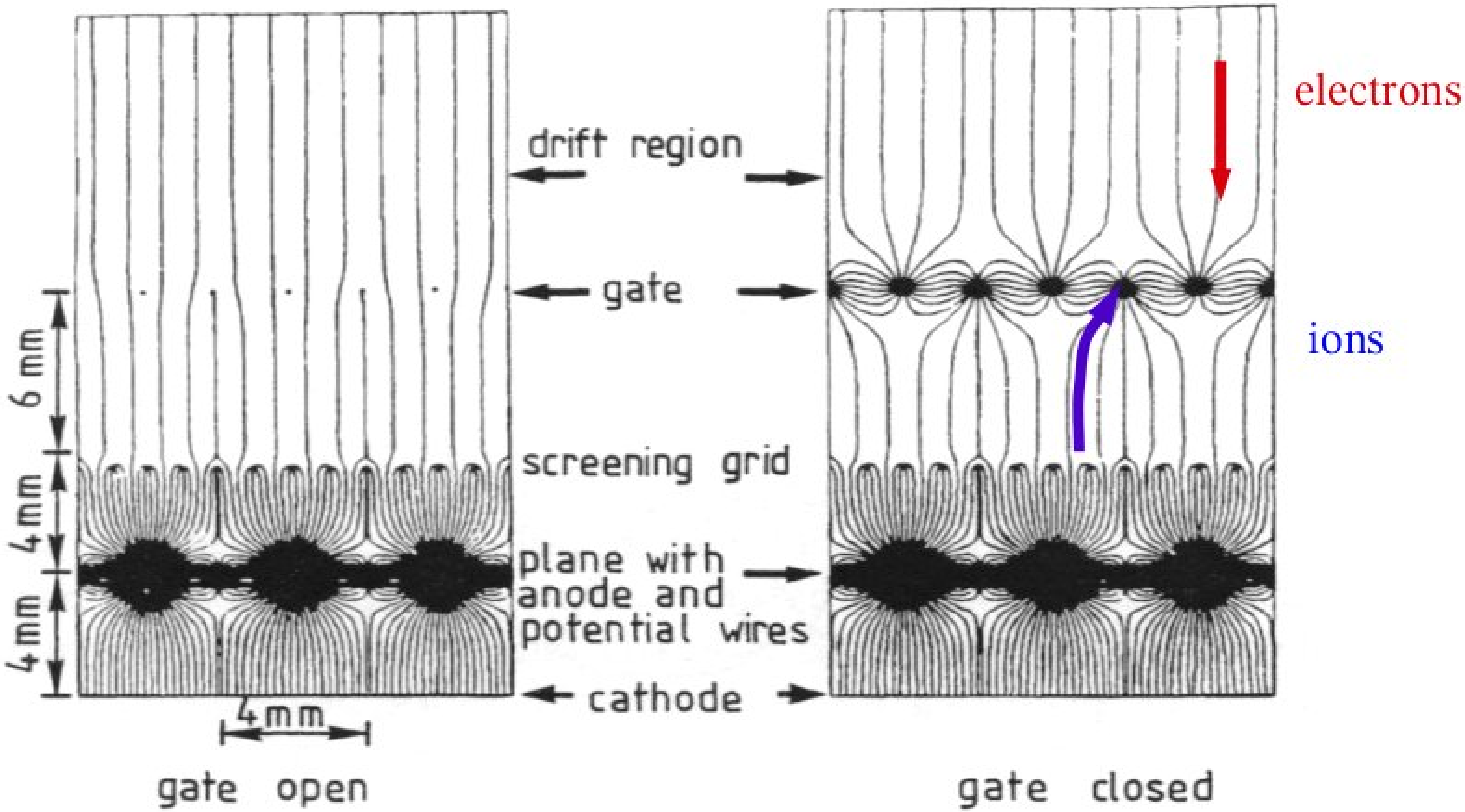

upon interaction trigger switch gating grid to 'open' for max drift time, then close again
$\rightarrow$ all ions from amplification drift toward gating grid and do not enter drift region.

example: the ALICE TPC for LHC Pb + Pb collisions

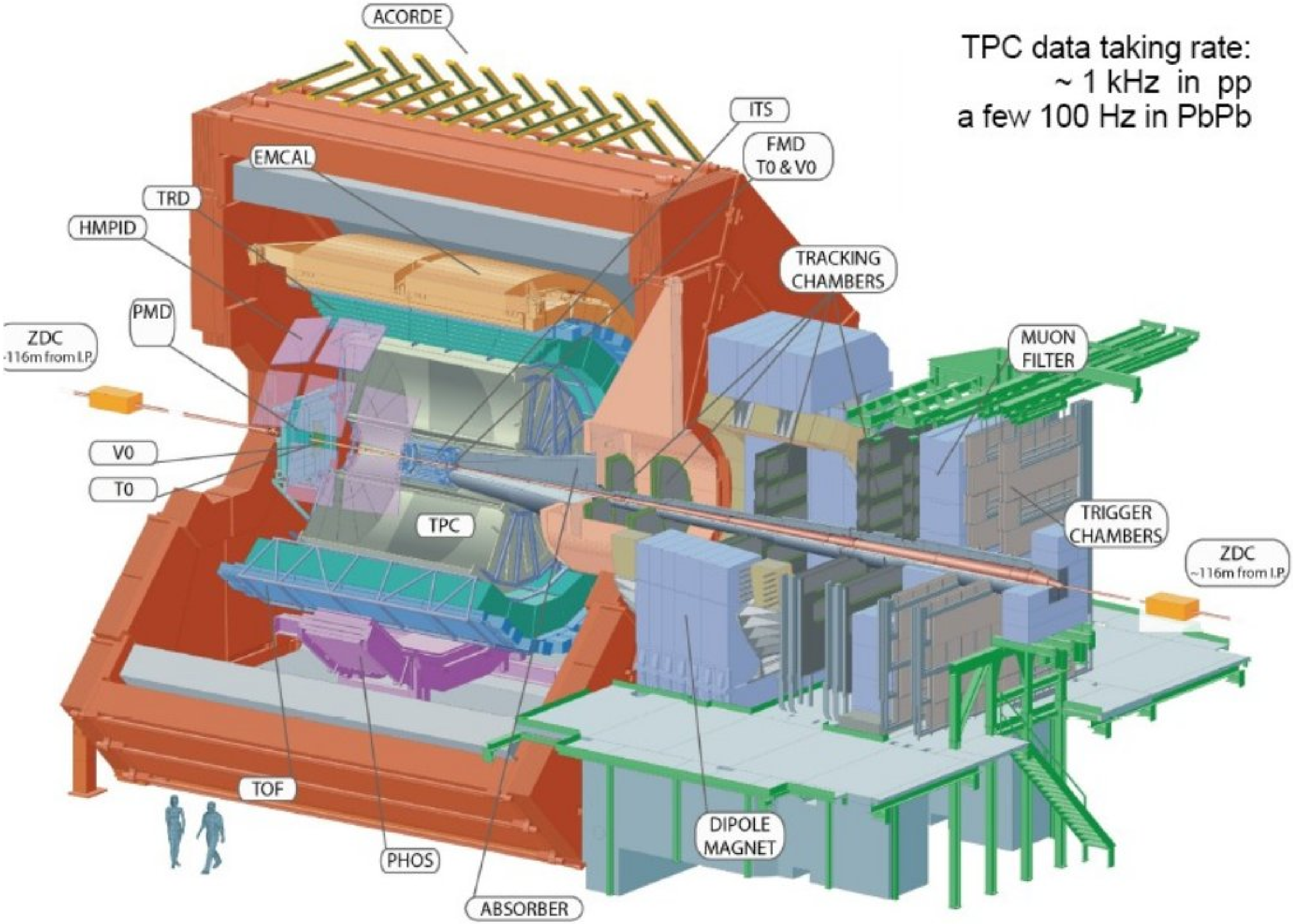

TPC data taking rate:
~ 1 kHz in pp
a few 100 Hz in PbPb

example: the ALICE TPC for LHC Pb + Pb collisions

the challenge:
identification and reconstruction of 5000 (up to 15000) tracks of charged particle in one event

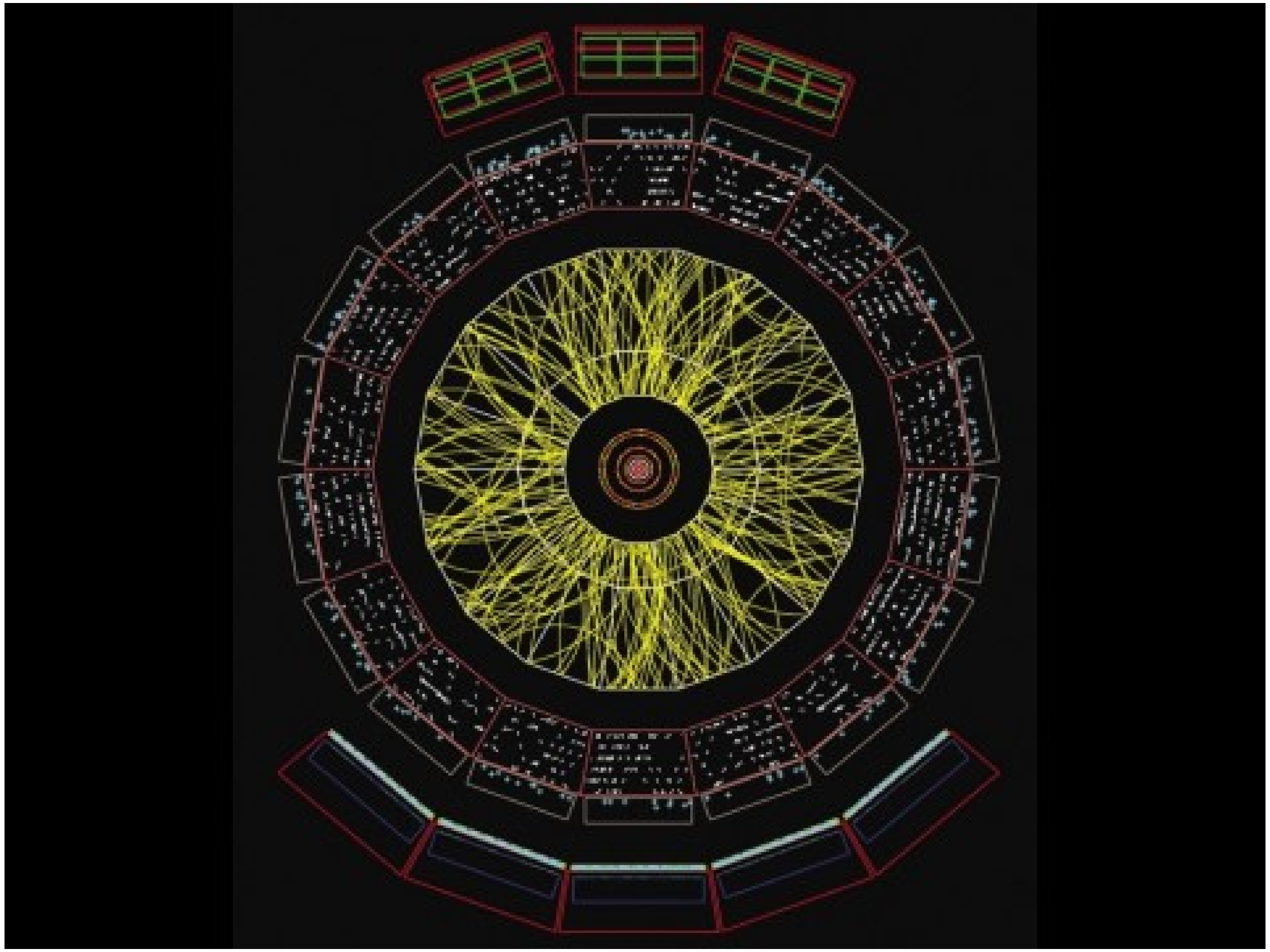

cut through central barrel of ALICE:
tracks of charged particles in a 1 degree segment in θ (1% of all tracks)

example: the ALICE TPC for LHC Pb + Pb collisions

challenges:

- very high multiplicity and desire for very good resolution
  - space charge
    - $\rightarrow$ optimize gating grid (even 1% leakage would be deadly)
    - $\rightarrow$ rate limitation, good luminosity monitoring
  - occupancy, want to keep it at inner radius below 40%
    - $\rightarrow$ optimize pad sizes and shapes (4 x 7.5 mm, total 558 000)
    - $\rightarrow$ 1000 time samples, 159 samples radially
- momentum resolution
  - low multiple scattering, small diffusion
    - $\rightarrow$ low Z cold gas Ne/CO_2 coupled with small drift cells (occupancy)
      temperature control to 0.1 K (even resistors need to be cooled)
      need to know electric field to 10^{-4} precision
    - $\rightarrow$ small amount of electron-ion pairs
    - $\rightarrow$ high gas gain of 10000
- event rate
  - limited by drift time (cold gas and not more than 100 kV, 90 μs)
  - data volume (1 central collision 60 MByte, can't store much more than a few GByte/s)

technical specs:

$r = 0.85 - 2.47$ m, length 2 x 2.5 m, material budget 3.5% X_0

approximate performance:

$\sigma(p)/p = 1\%\ p$, efficiency 97%, $\sigma_{\mathrm{d}E/\mathrm{d}x}/(\mathrm{d}E/\mathrm{d}x) \leq 6\%$, 100-200 Hz event rate inside the field cage:

The TPC (Time Projection Chamber) – 3D reconstruction of up to 15 000 charged particle tracks per event

with 95 m^3 largest TPC ever built

central HV electrode 100 kV

field cage: voltage divider with E-field homogeneity of 10^{-4}

in the end caps: 72 multi-wire proportional chambers with cathode pad read-outs

560 million pixels!
precision better than 500 μm in all 3 dimensions, 159 points per track

Construction of multi-wire proportional chambers, 3 wire planes plus cathode pad read-out

at GSI, Phys. Inst. U. Heidelberg. U. Bratislava

challenge: small spacings, high gas gain, high geometrical precision

Pad Plane: 5504 pads (4 x 7.5 mm)

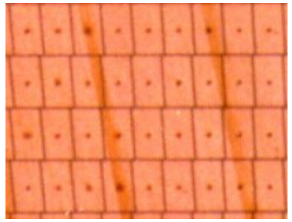

Close-up on the pads

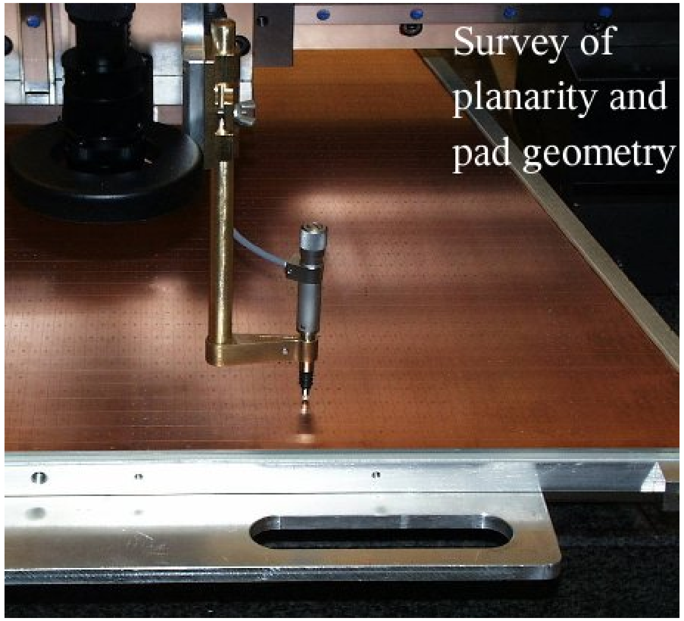

TPC Front End Electronics – 2 ASICS developed at Phys. Inst. U.Heidelberg and CERN, cooperation with ST Microelectronics

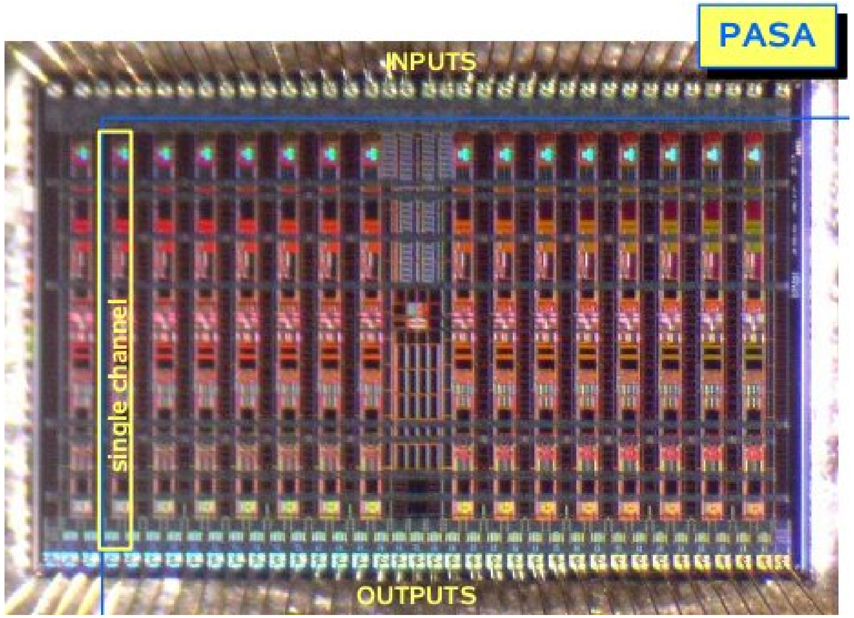

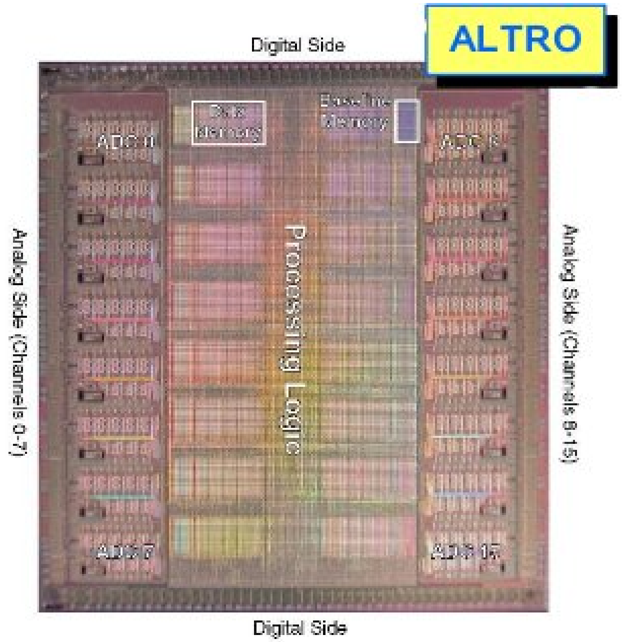

excellent performance (now also used by STAR at RHIC)

PASA: low noise preamplifier/shaper

ALTRO: commercial ADC (ST) **in same custom chip** with digital signal processing

electronics needs to be clever:
- zero suppression
- base line restoration
- etc. $\rightarrow$ put a lot of intelligence into digital chip after ADC, the ALTRO

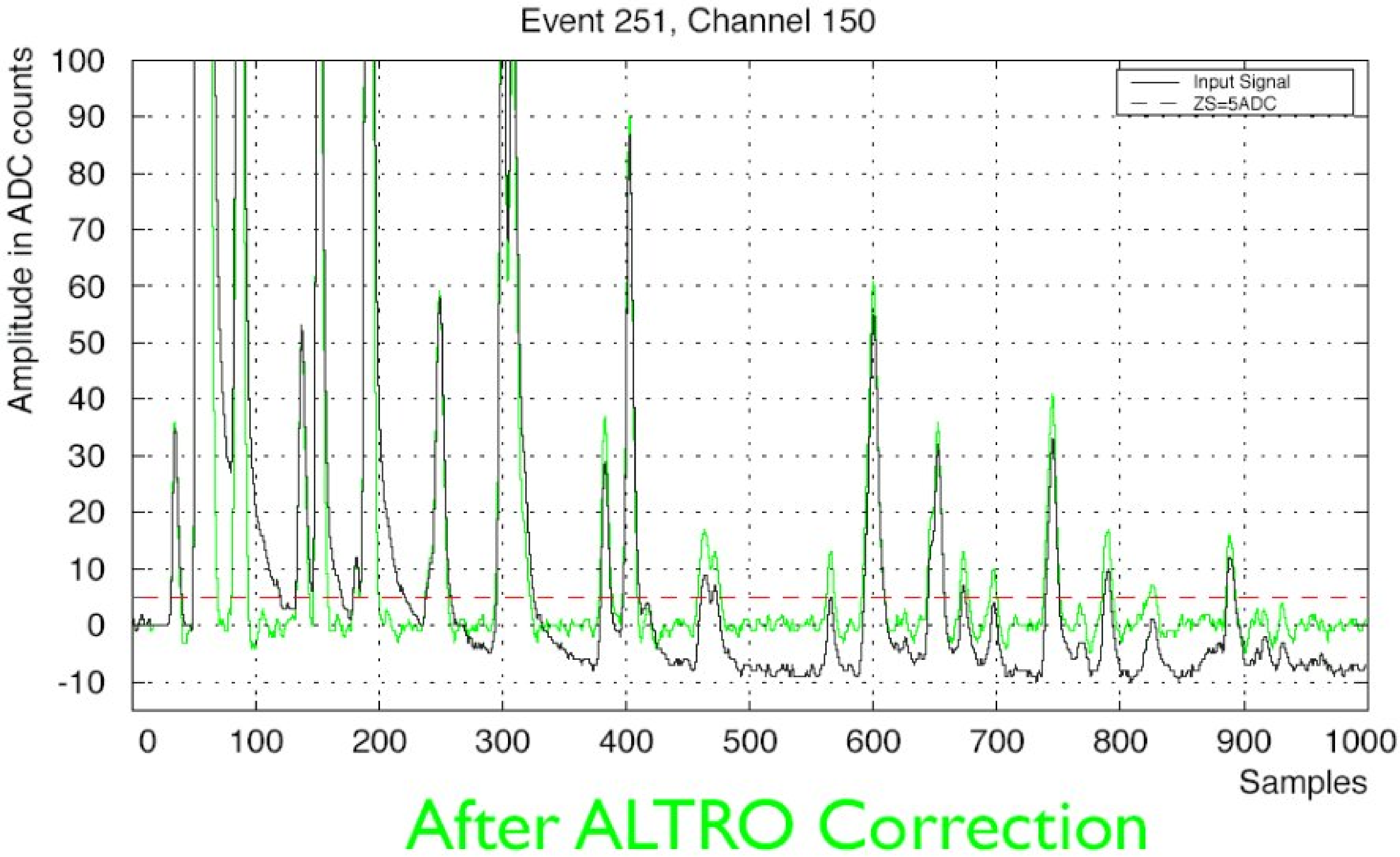

ALICE TPC: drift velocity

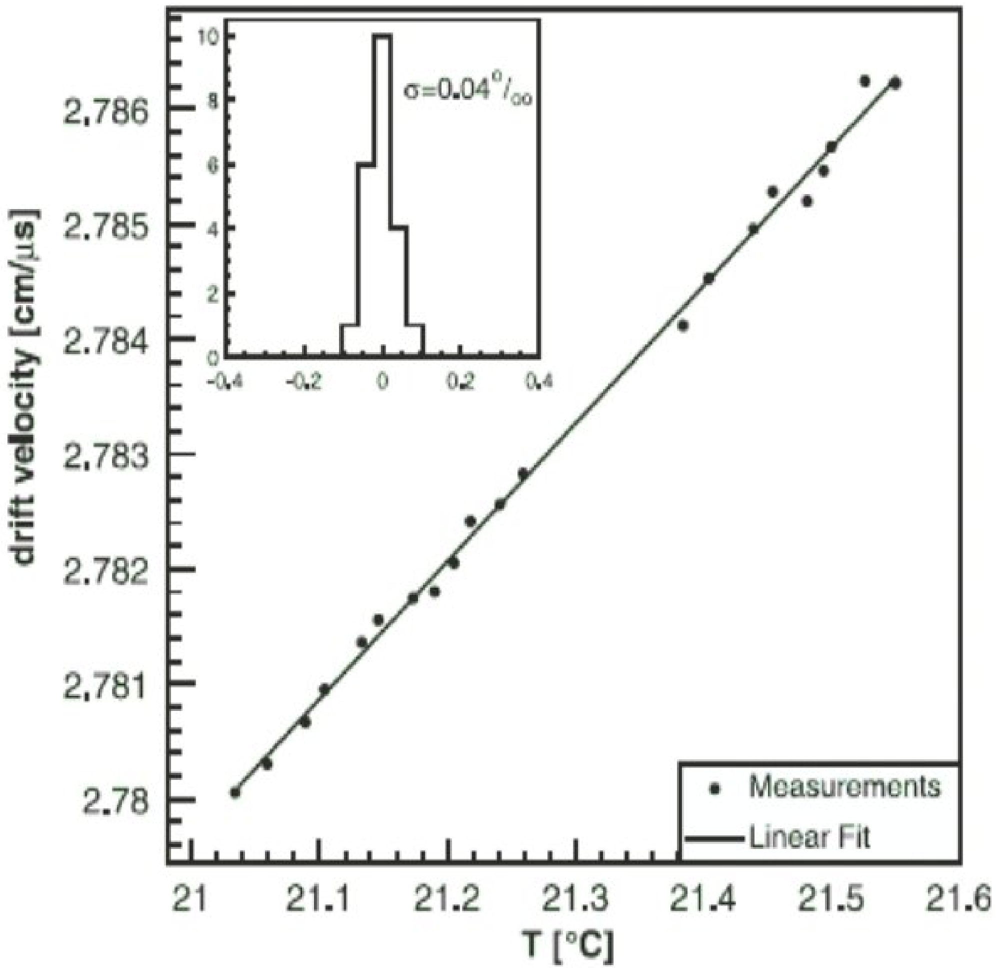

converts time into z coordinate
extreme precision needed . . .
measured with a small TPC
(using laser for gas ionization)

J. Wiechula et al., NIM A 548 (2005) 582

requires temperature stability of 0.1 K
TPC FEE dissipates 27 kW
TRD as direct neighbor 60 kW
60 independent cooling circuits
500 temperature sensors

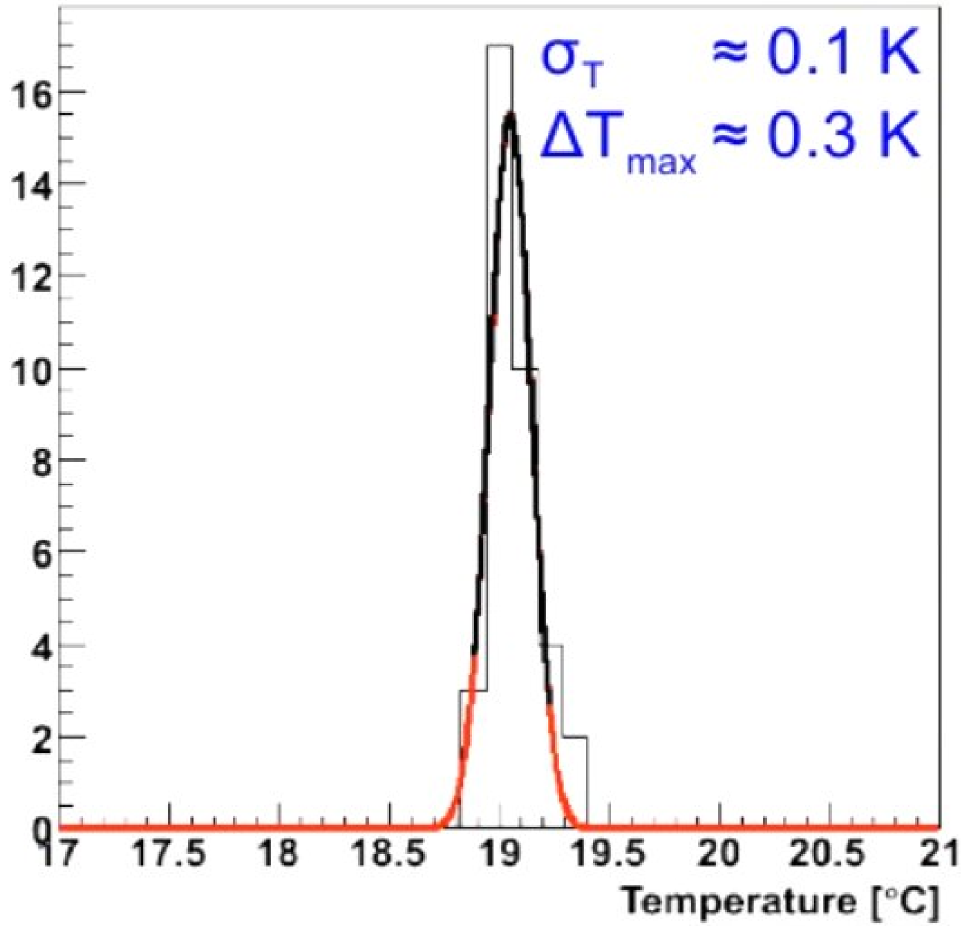

Performance of the ALICE TPC: particle identification

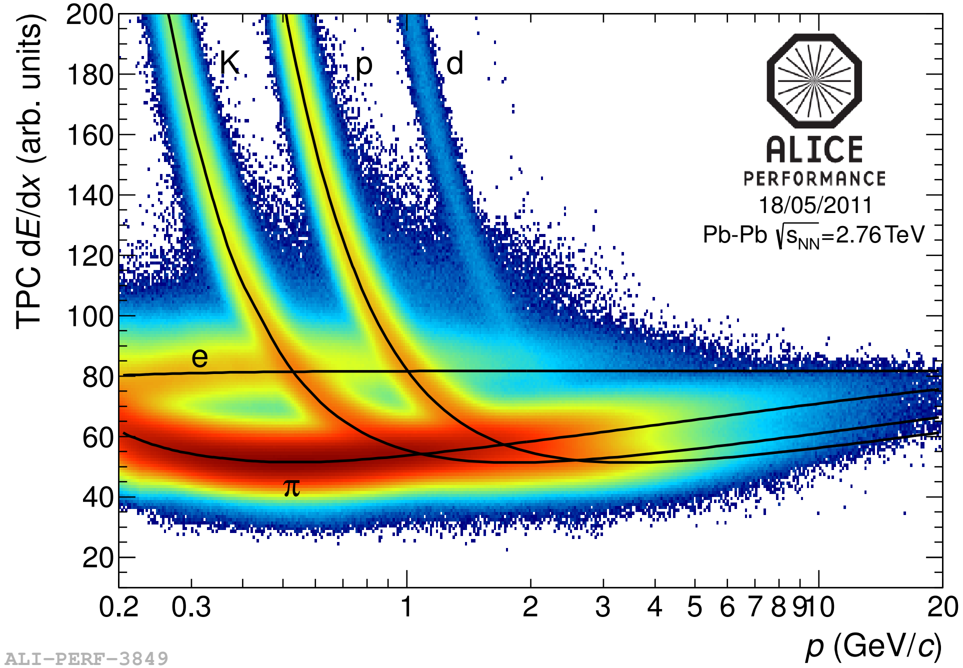

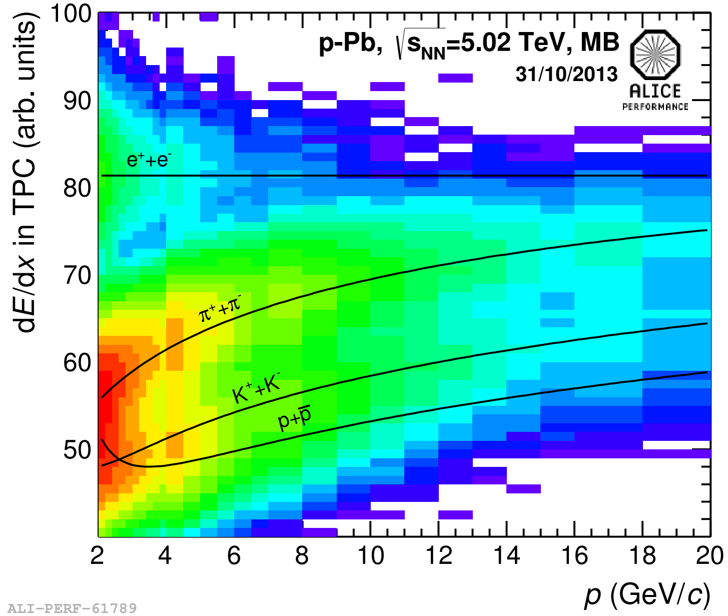

$$\frac{\sigma(\mathrm{d}E/\mathrm{d}x)}{\mathrm{d}E/\mathrm{d}x} = 5.2\% \text{ to } 6.5\%$$

(pp to central Pb-Pb)

crossings: use of TOF to resolve ambiguity

statistical separation possible even in relativistic rise region

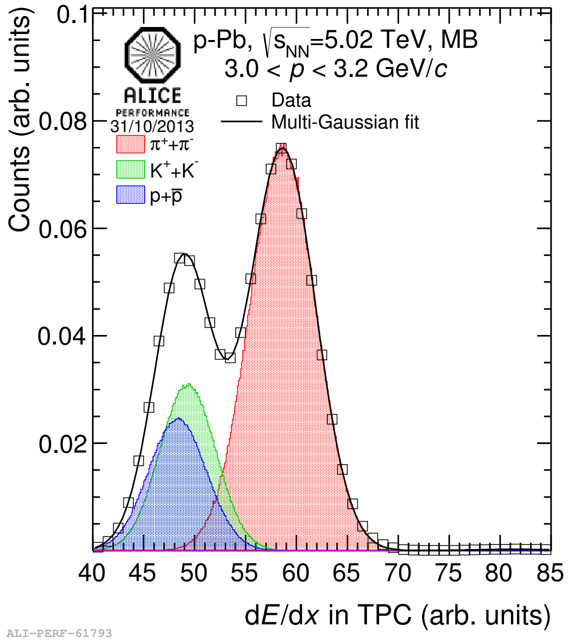

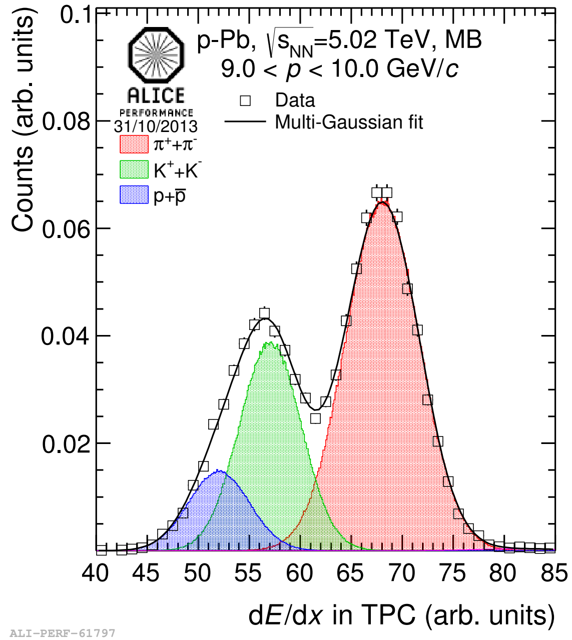

Performance of the ALICE TPC: momentum resolution

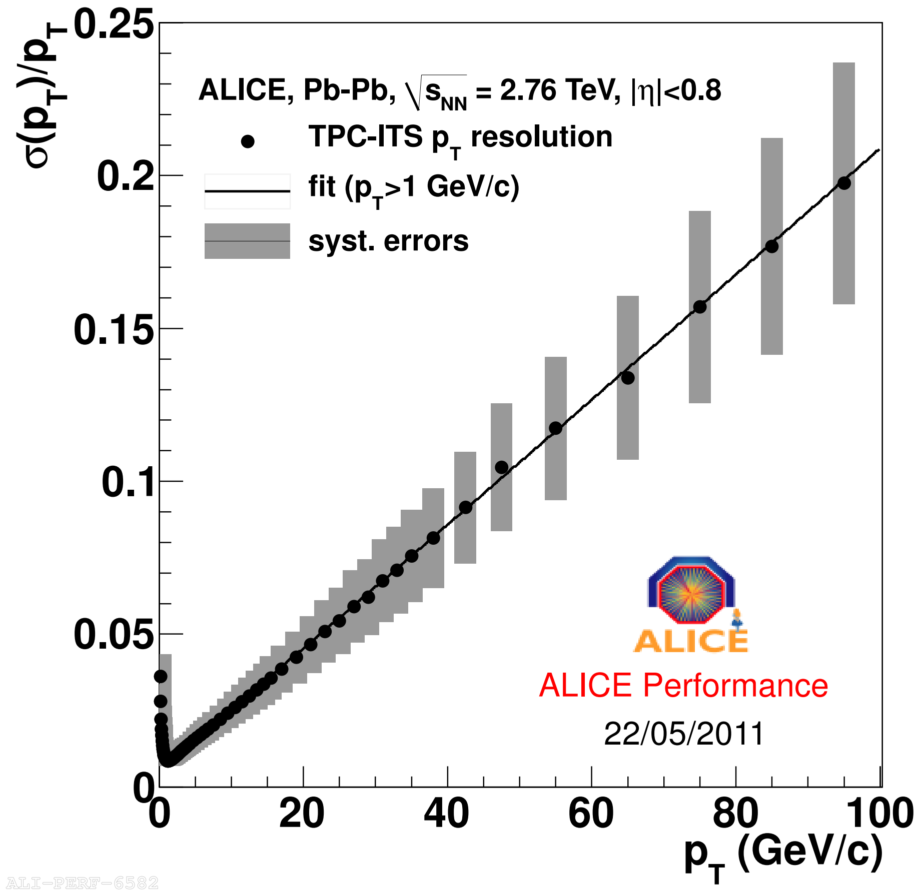

TPC standalone $p_\perp$-resolution

resolution at large $p_\perp$ is improved by a factor of about 3 if vertex is included in fit

further improvement by inclusion of track segments of Inner Tracker System and Transition Radiation Detector

TPC fully instrumented and installed in ALICE on Jan. 6, 2007

laser tracks

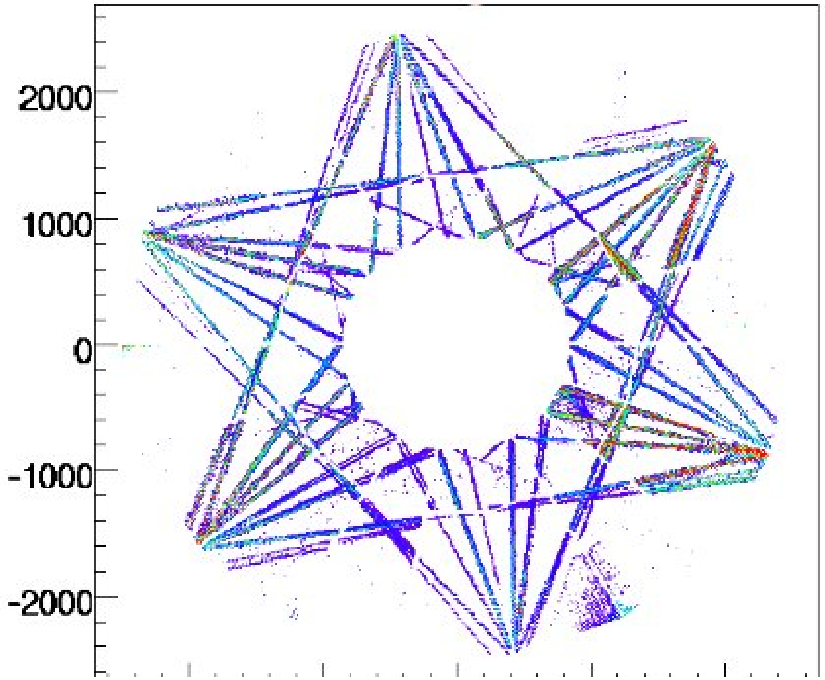

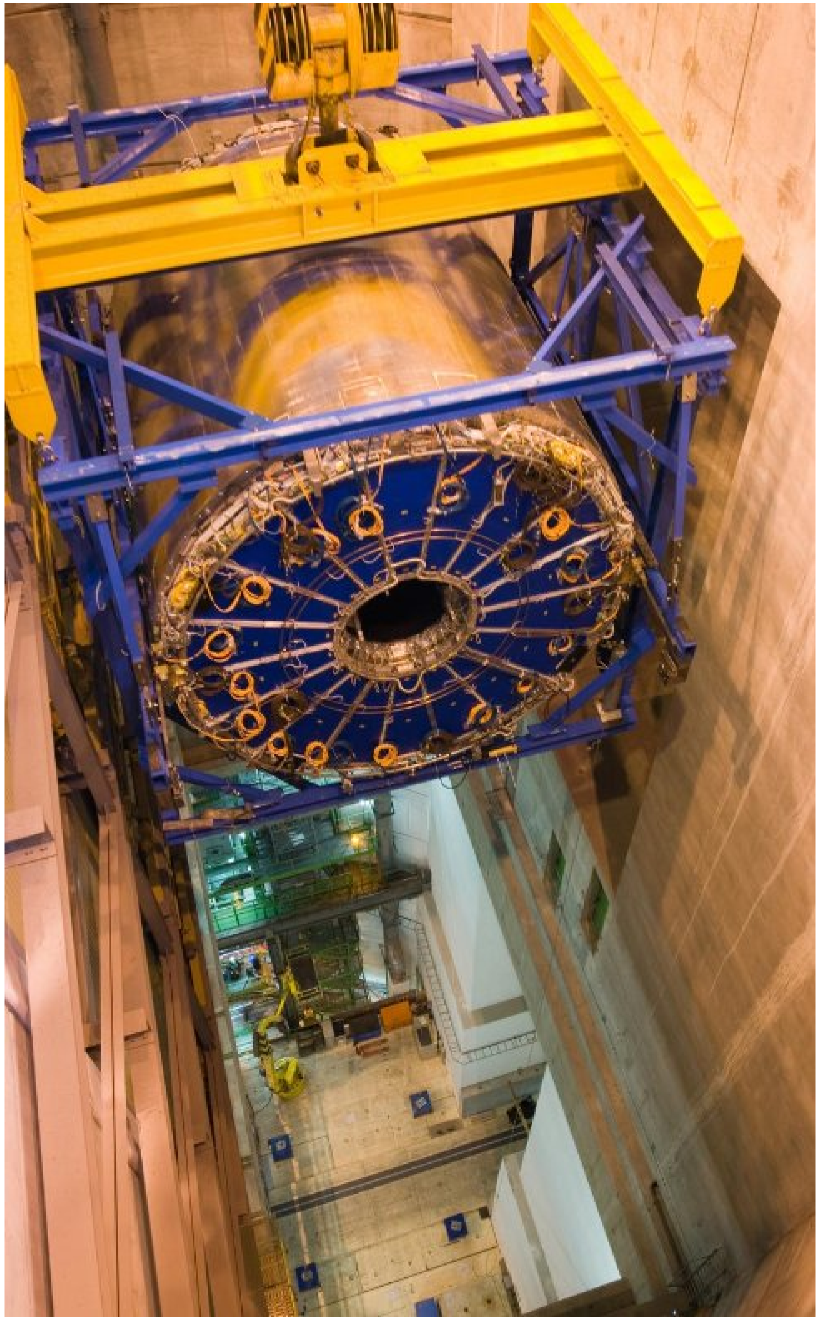

ALICE TPC up and running